LETTER

doi:10.1038/nature21406

Phosphatidylinositol 3-kinase δ blockade increases genomic instability in B cells

Mara Compagno[1]*, Qi Wang[1]*, Chiara Pighi[1]*, Taek-Chin Cheong[1], Fei-Long Meng[2]†, Teresa Poggio[3], Leng-Siew Yeap[2]†, Elif Karaca[1], Rafael B. Blasco[1], Fernanda Langellotto[1]†, Chiara Ambrogio[4], Claudia Voena[1,3], Adrian Wiestner[5], Siddha N. Kasar[4], Jennifer R. Brown[4], Jing Sun[4], Catherine J. Wu[4], Monica Gostissa[2]†, Frederick W. Alt[2] & Roberto Chiarle[1,3]

Activation-induced cytidine deaminase (AID) is a B-cell-specific enzyme that targets immunoglobulin genes to initiate class switch recombination and somatic hypermutation[1]. In addition, through off-target activity, AID has a much broader effect on genomic instability by initiating oncogenic chromosomal translocations and mutations involved in the development and progression of lymphoma[2]. AID expression is tightly regulated in B cells and its overexpression leads to enhanced genomic instability and lymphoma formation[3]. The phosphatidylinositol 3-kinase δ (PI3Kδ) pathway regulates AID by suppressing its expression in B cells[4]. Drugs for leukaemia or lymphoma therapy such as idelalisib, duvelisib and ibrutinib block PI3Kδ activity directly or indirectly[5–8], potentially affecting AID expression and, consequently, genomic stability in B cells. Here we show that treatment of primary mouse B cells with idelalisib or duvelisib, and to a lesser extent ibrutinib, enhanced the expression of AID and increased somatic hypermutation and chromosomal translocation frequency to the *Igh* locus and to several AID off-target sites. Both of these effects were completely abrogated in AID-deficient B cells. PI3Kδ inhibitors or ibrutinib increased the formation of AID-dependent tumours in pristane-treated mice. Consistently, PI3Kδ inhibitors enhanced AID expression and translocation frequency to *IGH* and AID off-target sites in human chronic lymphocytic leukaemia and mantle cell lymphoma cell lines, and patients treated with idelalisib, but not ibrutinib, showed increased somatic hypermutation in AID off-targets. In summary, we show that PI3Kδ or Bruton's tyrosine kinase inhibitors increase genomic instability in normal and neoplastic B cells by an AID-dependent mechanism. This effect should be carefully considered, as such inhibitors can be administered to patients for years.

We first tested the effects of PI3Kδ blockade in primary mouse B cells stimulated with anti-CD40 and interleukin (IL)-4 to undergo class switch recombination (CSR)[9]. In these cells, the PI3Kδ inhibitor idelalisib or the dual PI3Kγδ inhibitor duvelisib accelerated and increased AID induction, whereas the PI3Kγ inhibitor AS-604850 did not affect AID abundance (Fig. 1a). Consistently, AID mRNA levels were significantly enhanced by either idelalisib or duvelisib (Fig. 1b). To more precisely define transcription changes of AID in activated mouse B cells treated with PI3Kδ inhibitors, we performed global run-on sequencing (GRO-seq) analysis[9]. Of the five enhancers associated with the *Aicda* gene, we found a substantial increase in both sense and antisense transcription in the E4 enhancer downstream of the transcription start site (TSS; Fig. 1c, d), consistent with the pattern of AID expression that we described in CSR-activated and germinal centre B cells[10]. As a result of the enhanced AID expression, idelalisib and duvelisib increased CSR to IgG_1 *in vitro* in activated B cells (Fig. 1e) as well as *in vivo* in germinal centre B cells (Extended Data Fig. 1a–c). The effects were significant at doses ranging from 0.1 μM to 1 μM, which encompass the plasma concentration of these drugs observed in patients[7,11] (Fig. 1e, Extended Data Fig. 1d–f). Idelalisib and duvelisib reduced proliferation of B cells, whereas AS-604850 did not (Extended Data Fig. 1g), demonstrating that PI3Kδ blockade enhanced AID expression and CSR despite inhibition of B-cell proliferation[12]. In a reverse genetic experiment, B cells expressing a PI3Kδ gain-of-function mutant (PI3Kδ(E1021K)) recently discovered in patients with immunodeficiency and impaired CSR[13,14], showed decreased AID mRNA and protein levels as well as CSR (Extended Data Fig. 1h–j).

Because AID induces DNA damage and chromosomal translocations at defined on-target (*Igh* locus) and off-target (non-*Igh* locus) genomic sites[1,9,15], we next analysed whether the enhanced AID expression induced by PI3Kδ blockade would result in increased genome instability. We applied high-throughput genome-wide translocation sequencing (HTGTS)[9] to generate genomic maps of chromosomal translocations in activated mouse B cells treated with idelalisib or duvelisib. By this approach, we sequenced thousands of translocation junctions between endogenous double-strand breaks (DSBs) and a *c-myc* DSB initiated by the I-SceI nuclease[9] (Supplementary Table 1). Overall, idelalisib or duvelisib similarly increased the formation of translocation junctions between *c-myc* and AID on-target sites in the *Igh* locus or AID off-target sites in the genome (Fig. 2a–c). In the *Igh* locus, translocation junctions increased and clustered in the Sμ, Sγ1 and Sε regions, as previously described[9,15] (Extended Data Fig. 2a, b). In addition, the number of AID off-target sites in B cells treated with idelalisib or duvelisib, but not AS-604850, was substantially increased (Fig. 2c, Supplementary Table 2). AID off-target sites induced by PI3Kδ blockade were widely dispersed across the genome (Extended Data Fig. 2c, d), were largely overlapping with AID off-target sites previously identified by HTGTS[16], translocation capture sequencing[15], AID chromatin immunoprecipitation with DNA sequencing (ChIP–seq)[17] and replication protein A (RPA)-ChIP[18] (Supplementary Table 2), and included *Aicda* itself and several genes involved in recurrent translocations in human lymphomas, such as *Pax5, Pim1, Bcl6, Il21r* and *Bcl2l1* (Extended Data Fig. 2c–e). The median fold change translocation frequency was 2.0 and 2.6 for AID on-target sites and 4.3 and 4.7 for AID off-target sites for idelalisib or duvelisib, respectively, with 95th percentiles up to 12.9 and 17.0 fold changes for idelalisib or duvelisib (Fig. 2d). Both on-target and off-target translocation junctions were almost completely abrogated in AID-deficient B cells, thus demonstrating that the increased genomic instability induced by PI3Kδ blockade was

[1]Department of Pathology, Children's Hospital Boston and Harvard Medical School, Boston, Massachusetts 02115, USA. [2]Howard Hughes Medical Institute, Program in Cellular and Molecular Medicine, Boston Children's Hospital, and Department of Genetics, Harvard Medical School, Boston, Massachusetts 02115, USA. [3]Department of Molecular Biotechnology and Health Sciences, University of Torino, Torino 10126, Italy. [4]Department of Medical Oncology, Dana-Farber Cancer Institute, Harvard Medical School, Boston, Massachusetts 02115, USA. [5]Hematology Branch, National Heart, Lung, and Blood Institute, Bethesda, Maryland, USA. †Present addresses: Institute of Biochemistry and Cell Biology, Shanghai Institutes for Biological Sciences, Chinese Academy of Sciences, Shanghai 200031, China (F.-L.M.); Shanghai Institute of Immunology, Shanghai Jiao Tong University School of Medicine, Shanghai 200025, China (L.-S.Y.); Agenus Inc., 3 Forbes Road, Lexington, Massachusetts 02421, USA (F.L., M.G.).
*These authors contributed equally to this work.

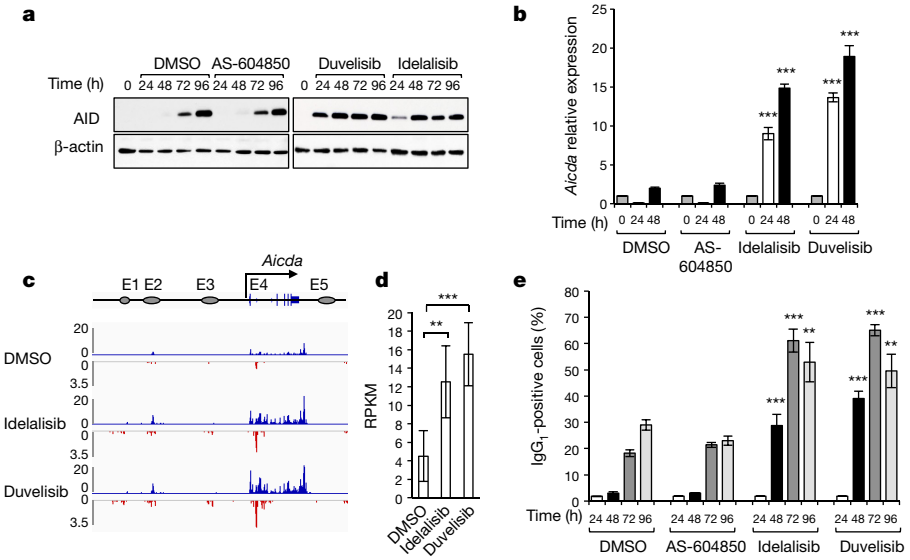

Figure 1 | PI3Kδ blockade increases AID expression and CSR in activated mouse B cells. a, Western blot for AID protein from B cells treated with the indicated inhibitors (1 μM) ($n = 3$ biological replicates). For gel source data, see Supplementary Fig. 1. **b**, *Aicda* mRNA levels were analysed by RT–qPCR. **c**, GRO-seq profiles of *Aicda* gene in B cells at 48 h after activation ($n = 2$ biological replicates). Blue profiles, sense transcription; red profiles, antisense transcription. **d**, Quantification of GRO-seq sense and antisense reads per kilobase per million mapped reads (RPKM) in the *Aicda* gene, $^{**}P \leq 0.01$,$^{***}P \leq 0.001$, multiple test adjusted. **e**, IgG_1 CSR in activated B cells. Data are expressed as mean ± s.d. ($n = 3$ biological replicates); $^{**}P \leq 0.01$, $^{***}P \leq 0.001$, two-tailed Student's *t*-test from idelalisib- or duvelisib- versus DMSO-treated B cells (**b**, **d**).

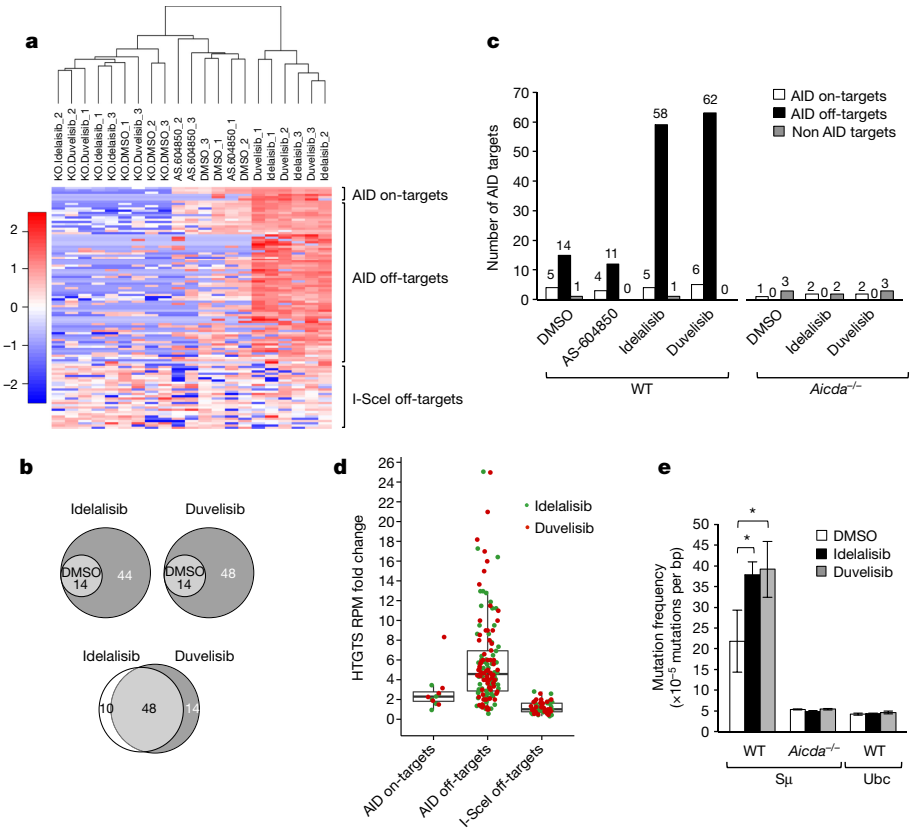

Figure 2 | PI3Kδ blockade increases the frequency of genome-wide chromosomal translocations in activated mouse B cells. a, Hierarchical clustering of translocation frequency analysis of HTGTS libraries generated from wild-type and $Aicda^{-/-}$ B cells treated with the indicated inhibitors. AID on-target (*Igh* and *Igk* loci) and off-target are listed in Supplementary Table 2. I-SceI off-targets are listed in Extended Data Fig. 3d. **b**, Venn diagrams showing the fraction of shared AID off-targets. **c**, Numbers of AID on-target (*Igh* and *Igk* loci) and off-target hot spots from wild-type and $Aicda^{-/-}$ B cells. Data pooled from at least $n = 3$ biological replicates (Supplementary Table 1). **d**, Fold change of HTGTS junction frequency in B cells treated with idelalisib or duvelisib compared to DMSO. I-SceI off-targets are used as an internal control for non-AID-mediated translocations. Whiskers extend to a maximum of 1.5× interquartile range beyond the box. **e**, Mutation frequency of the immunoglobulin Sμ region in wild-type and $Aicda^{-/-}$ B cells. Cumulative frequency of C-to-T or G-to-A transition mutations is indicated. Data are expressed as mean ± s.d. ($n = 3$ biological replicates). $^{*}P < 0.05$, two-tailed Student's *t*-test.

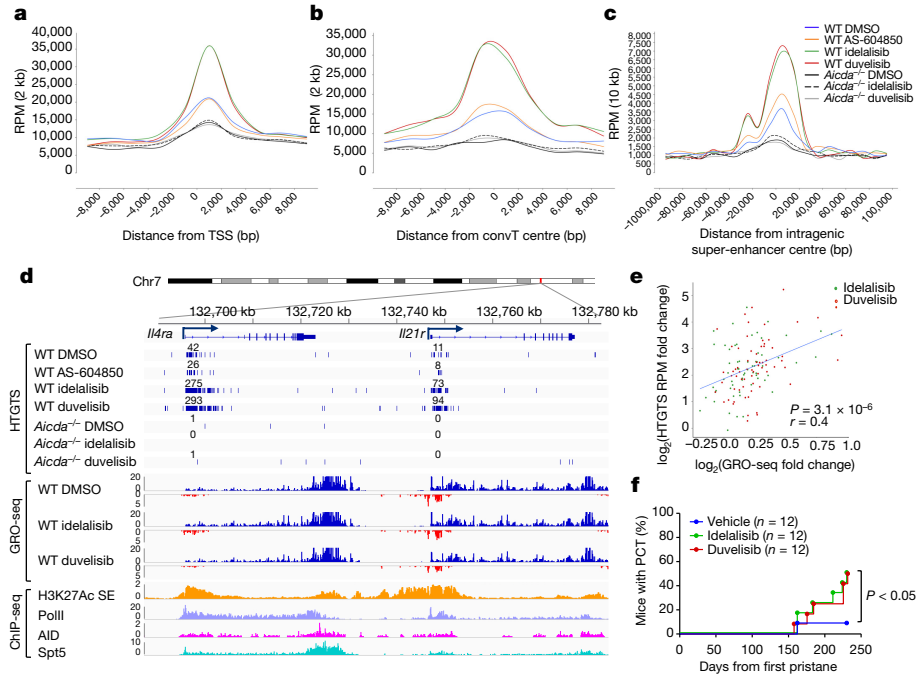

Figure 3 | Enhanced genomic instability in mouse B cells by PI3Kδ blockade. a–c, Genome-wide distribution of translocation junctions relative to TSS regions (**a**), convergent transcription (ConvT) regions (**b**) and intragenic super-enhancers (SEs) (**c**) in wild-type and *Aicda*$^{-/-}$ B cells treated with the indicated inhibitors. **d**, Detailed distribution of HTGTS junctions and GRO-seq reads in representative gene examples. Numbers of translocation junctions in focal clusters are indicated in bold. Corresponding Pol II, AID, Spt5 and H3K27Ac/SE ChIP–seq profiles are shown. **e**, Fold change HTGTS junctions plotted against GRO-seq transcription levels of AID targets in B cells treated with idelalisib or duvelisib over DMSO. Pearson's correlation coefficient; *P* value calculated by two-tailed *F*-test. **f**, Development of plasma cell tumour in mice induced with pristane and treated with idelalisib or duvelisib is plotted over time ($n = 12$ for each group in 2 independent cohorts of 6 mice). *P* values calculated by log-rank (Mantel–Cox) test.

AID-dependent (Fig. 2c, Extended Data Fig. 2). Conversely, on-target and off-target translocation junctions were significantly reduced in B cells expressing the PI3Kδ(E1021K) active mutant (Extended Data Fig. 3a–c). As a control, translocations to sites generated by the off-target activity of I-SceI that are independent of AID[9] showed no changes in B cells treated with idelalisib or duvelisib (Extended Data Fig. 3d, e).

Next, we investigated whether PI3Kδ blockade would also increase AID-mediated somatic hypermutation (SHM). Treatment with idelalisib or duvelisib significantly increased SHM in the Sμ region in wild-type but not AID-deficient activated B cells and had no effect on the *Ubc* promoter, a site previously shown to lack AID-mediated SHM[18] (Fig. 2e). Furthermore, PI3Kδ blockade increased 2.7- to 4.6-fold the mutation frequency at the V exon in activated B cells from mice with a VB1-8 exon in the productive allele[19] (Extended Data Fig. 4a–d). Therefore, we concluded that PI3Kδ blockade increased both AID-dependent chromosomal translocation formation and SHM in activated mouse B cells.

The current consensus is that AID preferentially targets genomic regions associated with high transcriptional activity, more frequently embedded within super-enhancers (SEs)[10,18]. SE regions typically are associated with events that direct AID binding and activity, such as RNA polymerase II (Pol II) transcriptional stalling with Spt5 accumulation[20], foci of convergent transcription (ConvT)[10] and non-coding RNA transcription[21]. In activated B cells treated with idelalisib or duvelisib, increased translocation junctions clustered 1–2 kb downstream of the TSS (Fig. 3a), peaked around ConvT regions (Fig. 3b) and intragenic SEs (Fig. 3c), and were associated with AID, Pol II and Spt5 binding sites (Fig. 3d, Extended Data Fig. 2e). Overall these data show that PI3Kδ blockade increased the formation of translocations but did not change their pattern of distribution in the genome.

We previously showed that high RNA transcription levels are associated with increased AID off-target activity in B cells[10]. We analysed GRO-seq data in B cells treated with PI3Kδ inhibitors (Extended Data Fig. 4e, Supplementary Table 3) and found that translocation junction frequency positively correlated with transcription of AID targets (Fig. 3e), indicating that concomitant transcriptional changes induced by PI3Kδ blockade could influence translocation frequency in specific AID target sites.

To study the effect of PI3Kδ blockade on genomic instability *in vivo*, first we showed that both idelalisib and duvelisib significantly increased AID off-target activity at the endogenous *c-myc* locus in germinal centre B cells (Extended Data Fig. 5a, b). Next, we investigated the effects of PI3Kδ blockade in the pristane-induced plasma cell tumour model in which tumour formation is driven largely by AID-dependent *Igh–c-myc* translocations[22]. In this model, treatment with idelalisib or duvelisib significantly increased the frequency of plasma cell tumour formation (Fig. 3f, Extended Data Fig. 5c–f). Overall, these data indicate that PI3Kδ blockade enhances AID-mediated genomic instability and tumour formation *in vivo* in mice.

As PI3Kδ inhibitors have been recently approved for the treatment of B-cell malignancies, we next investigated whether PI3Kδ blockade also enhanced AID expression in human leukaemia/lymphoma B cells. Idelalisib and duvelisib, but not AS-604850, blocked the proliferation of chronic lymphocytic leukaemia (CLL) (MEC1), mantle cell leukaemia (Mino and JeKo-1) or B lymphoblastoid (GM06990) cell lines (Extended Data Fig. 6a), yet induced a significant increase in *AID* mRNA (Fig. 4a, b, Extended Data Fig. 6b) and protein expression (Fig. 4c, Extended Data Fig. 6c–e). To test whether enhanced AID expression by PI3Kδ blockade was sufficient to increase genomic instability, we introduced DSBs in the human *c-MYC* locus using CRISPR/Cas9 technology and adapted HTGTS to human B cells (Extended Data Fig. 7a, b). Translocation junctions induced by off-target Cas9 activity were easily identified as unique for each single guide RNA sequence in MEC1 and JeKo-1 cell lines, and were excluded from the analysis (Extended Data Fig. 7c–h). HTGTS not only identified the *IGH* locus as a target for recurrent translocations in both cell lines, but

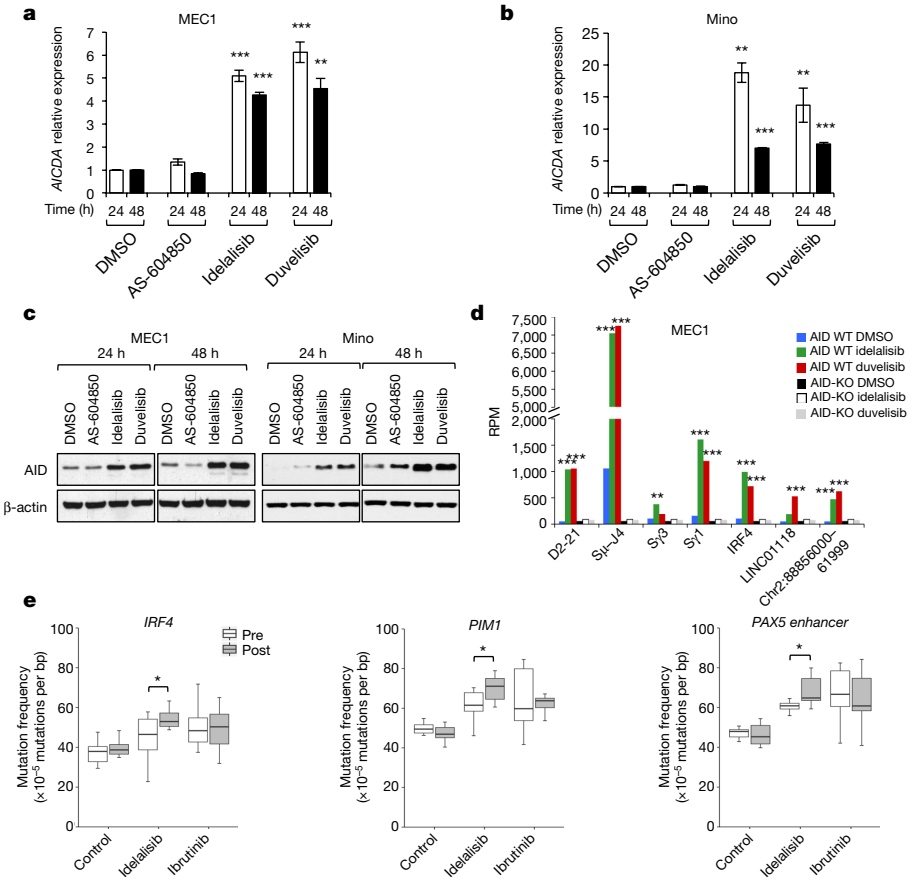

Figure 4 | PI3Kδ inhibitors increase AID expression and genomic instability in human B cells. a, **b**, *AICDA* mRNA relative expression in the human MEC1 or Mino B-cell lines treated with the indicated inhibitors (1 μM). Data are mean ± s.d. ($n = 3$ technical replicates, $n = 3$ biological replicates). $^{**}P \leq 0.01$, $^{***}P \leq 0.001$; two-tailed Student's *t*-test. **c**, Western blot for AID protein expression in MEC1 and Mino B-cell lines ($n = 4$ biological replicates). For gel source data, see Supplementary Fig. 1. **d**, Translocation junction frequency in AID on-target (D2-21 and Sμ–J4 region in the *IGH* locus) and AID off-target sites in MEC1 B-cell line treated with 1 μM DMSO, idelalisib or duvelisib. AID-knockout MEC1 cells were generated by CRISPR/Cas9-mediated deletion (Extended Data Fig. 8e). Data are from pooled HTGTS libraries from 3 independent experiments. **FDR ≤ 0.01, ***FDR ≤ 0.001. Statistical analysis in Methods. **e**, Mutation frequency calculated on the regions downstream TSS for *IRF4* and *PIM1*, and the *PAX5* enhancer region in patients with CLL treated with idelalisib or ibrutinib. Untreated patients with CLL are used as controls. Box plots indicate cumulative frequencies of C-to-T or G-to-A transition mutation in DNA samples collected before (pre) and after (post) treatment in each patient (control $n = 8$, idelalisib $n = 10$, ibrutinib $n = 10$; Supplementary Table 6). Whiskers extend to a maximum of 1.5× interquartile range beyond the box. $^{*}P < 0.05$, paired samples two-tailed Student's *t*-test.

also revealed translocations to recently identified AID off-targets in CLL and human lymphoma, such as *PIM1, IRF4, miR142* and *CXCR4* (refs 23–25). Remarkably, translocation to *IGH* as well as to AID off-targets were significantly increased by idelalisib and duvelisib treatment (Fig. 4d, Extended Data Fig. 8a–d, Supplementary Table 4), whereas no significant changes were observed in Cas9 off-targets that were used as internal control (Extended Data Fig. 7c–h). When we knocked-out AID in MEC1 cells by CRISPR/Cas9, chromosomal translocations to AID on- and off-targets were completely abrogated (Fig. 4d, Extended Data Fig. 8a, b, e). Thus, as in mouse B cells, PI3Kδ blockade also enhanced genomic instability by increasing AID expression in malignant human B cells.

Together with PI3Kδ inhibitors, drugs that block the Bruton's tyrosine kinase activity, such as ibrutinib, have been approved for the treatment of CLL and mantle cell lymphoma[5,26]. Because Bruton's tyrosine kinase modulates PI3K signalling[27], as shown by the block of AKT phosphorylation induced by ibrutinib in B cells (Extended Data Fig. 9a, b), we asked whether AID expression and genomic instability were also increased by ibrutinib. In CSR-activated mouse B cells, ibrutinib reduced cell proliferation, yet enhanced AID mRNA and protein levels as well as CSR (Extended Data Fig. 9c–f). Importantly, ibrutinib treatment increased translocation junctions to *Igh* and AID off-targets similarly although less potently than PI3Kδ inhibitors (Extended Data Figs 2a, e, 9g, h, Supplementary Table 5) and increased the frequency of plasma cell tumour formation in pristane-treated mice (Extended Data Fig. 5). In human B cells, ibrutinib reduced cell proliferation (Extended Data Fig. 6a), yet significantly enhanced AID expression (Extended Data Fig. 10a, b) as well as the frequency of translocation junctions to AID on-target and off-target sites (Extended Data Fig. 10c, Supplementary Table 4).

Finally, we investigated whether evidence for an increased AID activity could be found in patients treated with idelalisib or ibrutinib. We collected samples from patients with CLL treated for several months with either idelalisib or ibrutinib and analysed the frequency of SHM in known AID off-target genes by paired comparison of samples before and after treatment. A significant increase of SHM frequency was found in the regions downstream of the TSS of *IRF4* and *PIM1* genes and in the *PAX5* enhancer region (all known AID off-targets[24]), in patients treated with idelalisib but not in untreated or ibrutinib-treated patients; no increased SHM was found in a series of control genes (Fig. 4e, Extended Data Fig. 10d, Supplementary Table 6).

Overall, we provide evidence that PI3Kδ blockade enhances genomic instability in normal and malignant B cells by increasing AID levels. These findings have several potential implications. First, increased AID levels induced by PI3Kδ inhibitors could facilitate secondary oncogenic mutations or translocations in normal or malignant B cells in patients.

In this context, ibrutinib appears to have more limited effects, probably because of an indirect inhibition of the PI3K pathway. As AID activity is thought to have an important role in CLL biology as mutational signatures consistent with AID activity can be tracked in the evolution of CLL clones[28] and high AID expression in CLL is a poor prognostic factor[29], long-term monitoring for clonal evolution over time in patients on these drugs is essential, particularly given that current follow-up is very short. Furthermore, increased AID expression could accelerate resistance to targeted therapy through an increased mutational rate, as described for targeted therapies against BCR–ABL[30]. Finally, this work demonstrates the application of a genome-wide translocation assay to identify the genotoxic effects of drugs that were previously considered to be non-damaging to DNA.

Online Content Methods, along with any additional Extended Data display items and Source Data, are available in the online version of the paper; references unique to these sections appear only in the online paper.

Received 14 November 2016; accepted 20 January 2017.
Published online 15 February 2017.

1. Alt, F. W., Zhang, Y., Meng, F. L., Guo, C. & Schwer, B. Mechanisms of programmed DNA lesions and genomic instability in the immune system. *Cell* **152,** 417–429 (2013).
2. Nussenzweig, A. & Nussenzweig, M. C. Origin of chromosomal translocations in lymphoid cancer. *Cell* **141,** 27–38 (2010).
3. Robbiani, D. F. *et al.* AID produces DNA double-strand breaks in non-Ig genes and mature B cell lymphomas with reciprocal chromosome translocations. *Mol. Cell* **36,** 631–641 (2009).
4. Omori, S. A. *et al.* Regulation of class-switch recombination and plasma cell differentiation by phosphatidylinositol 3-kinase signaling. *Immunity* **25,** 545–557 (2006).
5. Byrd, J. C. *et al.* Targeting BTK with ibrutinib in relapsed chronic lymphocytic leukemia. *N. Engl. J. Med.* **369,** 32–42 (2013).
6. Gopal, A. K. *et al.* PI3Kδ inhibition by idelalisib in patients with relapsed indolent lymphoma. *N. Engl. J. Med.* **370,** 1008–1018 (2014).
7. Brown, J. R. *et al.* Idelalisib, an inhibitor of phosphatidylinositol 3-kinase p110δ, for relapsed/refractory chronic lymphocytic leukemia. *Blood* **123,** 3390–3397 (2014).
8. Dong, S. *et al.* IPI-145 antagonizes intrinsic and extrinsic survival signals in chronic lymphocytic leukemia cells. *Blood* **124,** 3583–3586 (2014).
9. Chiarle, R. *et al.* Genome-wide translocation sequencing reveals mechanisms of chromosome breaks and rearrangements in B cells. *Cell* **147,** 107–119 (2011).
10. Meng, F. L. *et al.* Convergent transcription at intragenic super-enhancers targets AID-initiated genomic instability. *Cell* **159,** 1538–1548 (2014).
11. Advani, R. H. *et al.* Bruton tyrosine kinase inhibitor ibrutinib (PCI-32765) has significant activity in patients with relapsed/refractory B-cell malignancies. *J. Clin. Oncol.* **31,** 88–94 (2013).
12. Rush, J. S., Liu, M., Odegard, V. H., Unniraman, S. & Schatz, D. G. Expression of activation-induced cytidine deaminase is regulated by cell division, providing a mechanistic basis for division-linked class switch recombination. *Proc. Natl Acad. Sci. USA* **102,** 13242–13247 (2005).
13. Angulo, I. *et al.* Phosphoinositide 3-kinase δ gene mutation predisposes to respiratory infection and airway damage. *Science* **342,** 866–871 (2013).
14. Lucas, C. L. *et al.* Dominant-activating germline mutations in the gene encoding the PI(3)K catalytic subunit p110δ result in T cell senescence and human immunodeficiency. *Nat. Immunol.* **15,** 88–97 (2014).
15. Klein, I. A. *et al.* Translocation-capture sequencing reveals the extent and nature of chromosomal rearrangements in B lymphocytes. *Cell* **147,** 95–106 (2011).
16. Hu, J., Tepsuporn, S., Meyers, R. M., Gostissa, M. & Alt, F. W. Developmental propagation of V(D)J recombination-associated DNA breaks and translocations in mature B cells via dicentric chromosomes. *Proc. Natl Acad. Sci. USA* **111,** 10269–10274 (2014).
17. Yamane, A. *et al.* Deep-sequencing identification of the genomic targets of the cytidine deaminase AID and its cofactor RPA in B lymphocytes. *Nat. Immunol.* **12,** 62–69 (2011).
18. Qian, J. *et al.* B cell super-enhancers and regulatory clusters recruit AID tumorigenic activity. *Cell* **159,** 1524–1537 (2014).
19. Yeap, L. S. *et al.* Sequence-Intrinsic Mechanisms that Target AID Mutational Outcomes on Antibody Genes. *Cell* **163,** 1124–1137 (2015).
20. Pavri, R. *et al.* Activation-induced cytidine deaminase targets DNA at sites of RNA polymerase II stalling by interaction with Spt5. *Cell* **143,** 122–133 (2010).
21. Pefanis, E. *et al.* Noncoding RNA transcription targets AID to divergently transcribed loci in B cells. *Nature* **514,** 389–393 (2014).
22. Potter, M. Neoplastic development in plasma cells. *Immunol. Rev.* **194,** 177–195 (2003).
23. Pasqualucci, L. *et al.* Hypermutation of multiple proto-oncogenes in B-cell diffuse large-cell lymphomas. *Nature* **412,** 341–346 (2001).
24. Puente, X. S. *et al.* Non-coding recurrent mutations in chronic lymphocytic leukaemia. *Nature* **526,** 519–524 (2015).
25. Landau, D. A. *et al.* Mutations driving CLL and their evolution in progression and relapse. *Nature* **526,** 525–530 (2015).
26. Wang, M. L. *et al.* Targeting BTK with ibrutinib in relapsed or refractory mantle-cell lymphoma. *N. Engl. J. Med.* **369,** 507–516 (2013).
27. Burger, J. A. & Chiorazzi, N. B cell receptor signaling in chronic lymphocytic leukemia. *Trends Immunol.* **34,** 592–601 (2013).
28. Kasar, S. *et al.* Whole-genome sequencing reveals activation-induced cytidine eaminase signatures during indolent chronic lymphocytic leukaemia evolution. *Nat. Commun.* **6,** 8866 (2015).
29. Palacios, F. *et al.* High expression of AID and active class switch recombination might account for a more aggressive disease in unmutated CLL patients: link with an activated microenvironment in CLL disease. *Blood* **115,** 4488–4496 (2010).
30. Klemm, L. *et al.* The B cell mutator AID promotes B lymphoid blast crisis and drug resistance in chronic myeloid leukemia. *Cancer Cell* **16,** 232–245 (2009).

Supplementary Information is available in the online version of the paper.

Acknowledgements We thank K. Okkenhaug and F. Garcon for providing wild-type and mutated PI3Kδ constructs, F. Zhang for providing CRISPR/Cas9 plasmids. We thank M. Fleming and M. M. Awad for critically reading the manuscript. This work was supported by NIH grants R01 CA196703-01 to R.C.; 1U10CA180861-01 to C.J.W., R01AI077595 to F.W.A; Associazione Italiana per la Ricerca sul Cancro grant IG-12023 to R.C. and MFAG 10708 to M.C.; Worldwide Cancer Research grant 12-0216 to R.C.; Compagnia di San Paolo-Comitato Gigi Ghirotti to M.C.; American Cancer Society Grant RSG-13-002-01-CCE to J.R.B.; T.C.C. is supported by a National Research Foundation of Korea(NRF) fellowship; L.S.Y. was a Cancer Research Institute postdoctoral fellow; F.M. was a Lymphoma Research Foundation postdoctoral fellow; J.S. is a recipient of a PhRMA Foundation Research Fellowship; C.J.W. is Scholar of the Leukemia and Lymphoma Society; F.W.A. is an investigator of the Howard Hughes Medical Institute. A. W. is supported by the intramural program of NHLBI, NIH.

Author Contributions M.C. and C.P. planned and performed experiments. Q.W. performed analysis of the data. T.-C.C., F.L., T.P., C.A., C.V., and M.G. performed experiments. E.K. and R.B contributed to CRISPR/Cas9 experiments. F.M. performed GRO-seq experiments. L.-S.Y. performed the mutational analysis on VB1-8 exon. A.W., S.N.K, J.R.B, J.S., and C.J.W. provided clinical samples. F.W.A contributed to the design and interpretation of the experiments, and contributed to writing the manuscript. R.C. conceived and designed all the experiments, analysed data, and wrote the manuscript with the help of M.C., Q.W., and C.P. All authors discussed the results and commented on the manuscript.

Author Information Reprints and permissions information is available at www.nature.com/reprints. The authors declare competing financial interests: details are available in the online version of the paper. Readers are welcome to comment on the online version of the paper. Correspondence and requests for materials should be addressed to R.C. (roberto.chiarle@childrens.harvard.edu).

Reviewer Information *Nature* thanks D. Fruman and the other anonymous reviewer(s) for their contribution to the peer review of this work.

METHODS

Data reporting. No statistical methods were used to predetermine sample size.

PI3K inhibitors. Idelalisib (CAL-101, GS-1101; PI3Kδ inhibitor), duvelisib (IPI-145, INK1197; PI3Kγδ dual inhibitor), AS-604850 (PI3Kγ inhibitor) and ibrutinib (inhibitor of Bruton's tyrosine kinase) were purchased from Selleckchem and all used at 1 μM concentration in most experiments. In some experiments, inhibitors were used at 0.1 μM or 0.5 μM concentrations, as indicated in the corresponding figure legend.

Mice. Wild-type mice, *c-myc*$^{25\times\text{I-SceI}}$ and *c-myc*$^{25\times\text{I-SceI}}$*Aicda*$^{-/-}$ in the 129S2 mice background. All mice carrying the 25×I-SceI cassette were heterozygous for the modified *c-myc* allele containing the I-SceI cassette and were previously described[9,31]. At least three independent mice of the same sex (females) and similar age (8–12 weeks) were used for each experiment with B cells. No mice were excluded from the analysis and no randomization or blinding method was used. Animal experiments were performed under protocols approved by the Institutional Animal Care and Use Committee (IACUC) of Boston Children's Hospital (protocol 16-01-3093R) or by the Italian Ministry of Health for the University of Torino (approval no. 143/2013-B). They were housed and maintained in the specific-pathogen-free facility at Boston Children's Hospital.

Human leukaemia/lymphoma cell lines. Human leukaemia/lymphoma cell lines MEC1 (Chronic Lymphocytic Leukaemia), JeKo-1 and Mino (Mantle Cell Lymphoma), and GM06990 (EBV-immortalized lymphoblastoid B-cell line) were cultured in RPMI 1640 medium (Thermo Fisher Scientific) supplemented with 10% fetal bovine serum (FBS), penicillin-streptomycin (100 units per ml) and L-glutamine (2 mM). All cell lines tested negative for mycoplasma contamination. Cell lines were authenticated as they were purchased from ATCC (JeKo-1, Mino), DSMZ (MEC1) or the Coriell Institute (GM06990).

For experiments with PI3K inhibitors, cells were plated in 6-well plates at a concentration of 5×10^5 cells per ml. Cells were collected at the indicated time points for RNA or protein isolation or flow cytometry analysis or after 4 days of treatment to isolate genomic DNA for HTGTS libraries.

Samples from CLL patients. DNA before and after therapy from patients with CLL (untreated $n = 8$; idelalisib $n = 10$; ibrutinib $n = 10$; total 56 samples) was extracted from peripheral blood samples. Samples from idelalisib-treated patients were collected in the 99–224 CLL repository approved by the Dana-Farber Cancer Institute Institutional Review Board. Ibrutinib-treated patients were enrolled on a phase 2, open-label, single-centre, investigator-initiated study approved by the National Heart, Lung, and Blood Institutional Review Board at the National Institutes of Health (registered at http://www.clinicaltrials.gov, NCT01500733). All patients provided written informed consent. All cases were diagnosed according to the International guidelines and consented according to internal protocols. Details of treatment and sample collection for each patient are summarized in Supplementary Table 6.

B-cell purification and *ex vivo* activation. Splenic mouse B cells were isolated from mice by immunomagnetic depletion with anti-CD43 MicroBeads (Invitrogen) as previously described[9]. Briefly, all the non-B cells were depleted with anti-CD43 MicroBeads combined with Dynabeads Biotin Binder (Invitrogen); naive B cells were cultured at a concentration of 5×10^5 cells per ml in RPMI medium supplemented with 15% FBS, penicillin-streptomycin (100 units per ml), L-glutamine (2 mM), anti-CD40 (1 μg ml^{-1}, eBioscience) and recombinant mouse IL-4 (20 ng ml^{-1}; PeproTech). The purity of B-cell population was typically 96–98% in all experiments, as documented by flow cytometric analysis of B220 expression in enriched cells. Cells were collected after 4 days of treatment with inhibitors to isolate genomic DNA for HTGTS libraries and targeted re-sequencing experiments. For RNA and protein extraction, cells were collected at the indicated time points. Class switch recombination (CSR) was measured by staining with PE-labelled anti-mouse IgG_1 (BD Biosciences) and Cy5-PE-labelled anti-mouse B220 (eBiosciences). Data acquisition was performed using a FACSVerse flow cytometer (BD biosciences).

Mouse immunization and purification of germinal centre B cells. For immunization, sheep blood in Alsever's solution (BD) were washed with PBS and re-suspended in PBS at a concentration of 1×10^9 sheep red blood cells per ml. 8–12-week-old mice were immunized by intraperitoneal injection of 2×10^8 sheep red blood cells in a 200 ml volume. After 5 days, a booster injection was performed using fivefold more sheep red blood cells. On day 6 and for 7 consecutive days, animals were daily administered vehicle (0.5% carboxymethylcellulose, 0.05% Tween 80 in ultra-pure water) or idelalisib or duvelisib (10 mg per kg per day) by oral gavage. Spleens were collected at the end of treatment, placed on ice, washed in PBS to remove residual blood, cut into small pieces, crushed and physically dissociated using a Falcon cell strainer, and subjected to hypotonic lysis of erythrocytes. Mouse germinal centre B cells were isolated from the spleens of immunized mice by immunomagnetic depletion: first non-B-cells were depleted with anti-CD43 MicroBeads; next enriched B cells were incubated with a cocktail of biotinylated antibodies specific for CD11c (eBiosciences) and IgD (eBiosciences) to remove dendritic cells and mature naive B cells, respectively, as previously reported[32]. Enrichment of the germinal B cells was evaluated with PE-labelled anti-mouse GL7 (eBiosciences) and Cy5-PE-labelled anti-mouse B220 (eBiosciences).

Induction of plasma cell tumour in mice. 8-week-old female BALB/cAnNCrl mice were purchased from Charles River and housed in the University of Torino mouse facility under a protocol approved by the Italian Ministry of Health. Commercial pristane (2,6,10,14-tetramethylpentadecane) was purchased from Sigma. Pristane was administered by two 0.5 ml i.p. injections given 70 days apart, as previously described[22]. The mice were divided into four different groups: vehicle group (0.5% carboxymethylcellulose, 0.05% Tween 80 in ultra-pure water) and idelalisib or duvelisib or ibrutinib groups. Drugs were administered by oral gavage (10 mg per kg per day) for 70 days (5 days a week). Mice underwent follow-up assessment for the development of ascites and were killed when they reached a point of distress. Several tissues, including peritoneal tumour nodules, inflammatory granuloma, liver, spleen, intestine, were processed for histologic analysis. For histology, tissues and tumour nodules were fixed in 10% formalin over-night and transferred to 70% ethanol and embedded in paraffin. 4-μm-thick sections were stained with haematoxylin and eosin to evaluate the distribution of clusters of atypical plasma cells. Plasma cell tumours were diagnosed by finding clusters of 10 or more hyperchromatic, atypical plasma cells in hystology specimens, as previously reported[22].

PCR amplification of junction fragments in pristane experiment. PCR for *Igh–c-myc* translocations was performed on 500 ng of genomic DNA extracted from ascites by adapting protocols previously described[33,34]. Briefly, we performed two rounds of PCR with Phusion High-Fidelity DNA Polymerase (Thermo Fisher Scientific) using primers listed in Supplementary Table 7. All PCR reactions were performed with appropriate positive controls (genomic DNA obtained from mouse B cells activated *in vitro* and treated with PI3Kδ inhibitors) and negative controls (DNA from *Aicda*$^{-/-}$ mouse B cells). PCR conditions were 98 °C for 30 s followed by 25 cycles (98 °C, 10 s; 62 °C, 30 s; 72 °C, 4 min) for both the first and second round. PCR amplicons were purified and sequenced to confirm *Igh–c-myc* translocations.

Protein extraction and western blot analysis. Whole-cell extracts were obtained from purified mouse B cells or cell lines treated with 1 μM PI3K inhibitors using GST-FISH buffer (10 mM $MgCl_2$, 150 mM NaCl, 1% NP-40, 2% Glycerol, 1 mM EDTA, 25 mM HEPES (pH 7.5)) supplemented with protease inhibitors (Roche), 1 mM phenylmethanesulfonylfluoride (PMSF), 10 mM NaF and 1 mM Na_3VO_4. Extracts were cleared by centrifugation at 12,000 r.p.m. for 15 min. The supernatants were collected and assayed for protein concentration using the Bio-Rad protein assay method. 20 μg of proteins were loaded on 12% Mini-PROTEIN TGX gels (BIO-RAD), transferred on nitrocellulose membrane (GE Healthcare), blocked with 5% skimmed milk (BIO-RAD). Primary antibodies for immunoblotting included: rat monoclonal anti-mouse-AID (mAID-2 clone, eBioScience, catalogue no. 14-5959-82), mouse monoclonal anti-human-AID (ZA001, Life Technologies, catalogue no. 39-2500), rabbit monoclonal anti-PI3K π110δ (Ψ387, Abcam, catalogue no. 32401), rabbit polyclonal anti-β−actin (Sigma, catalogue no. A2066), rabbit monoclonal anti-phospho-AKT (S473) (D9E, Cell Signaling Technology, catalogue no. 4060), rabbit monoclonal anti-AKT (pan) (C67E7, Cell Signaling Technology, catalogue no. 4691). Membranes were developed with ECL solution (GE Healthcare). AID protein abundance was measured by ImageJ software and normalized for the β-actin intensity of the corresponding lane.

Quantitative RT–PCR analysis. Total RNA was isolated from primary mouse B cells and human lymphoma cells by TRIzol (Life Technologies). Before cDNA synthesis, 1 μg of total RNA was treated with 5 U μl^{-1} RNase-free recombinant DNase I (Roche). cDNA was transcribed using iScript cDNA synthesis kit following the manufacturer's instructions (Biorad). All quantitative RT–PCR experiments were performed in triplicate on ICycler iQ Real-Time PCR Detection System (Bio-Rad Laboratories) with SYBR green dye. Primer pairs are listed in Supplementary Table 7. Expression levels for individual transcripts were normalized against β-actin for murine samples or HuPO for human samples. Fold change in transcript levels were calculated as fold change over untreated cells.

Retroviral transduction of mouse primary B cells. Retroviral supernatants were prepared from Phoenix packaging cells transfected with retroviral vectors. The pMX-I-SceI vector has been previously described[9], PI3Kδ retroviruses (wild-type PI3K p110δ (denoted as p110δ^{WT}) and PI3K p110δ(E1021K)) were provided by K. Okkenhaug and F. Garcon (The Babraham Institute, UK)[13].

Briefly, Phoenix-ECO cells, a second-generation retrovirus-producer cell line, were maintained in Dulbecco's modified Eagle's medium (DMEM) supplemented with 10% FBS, penicillin-streptomycin (100 units per ml) and L-glutamine (2 mM). To generate retroviral particle, 3.5×10^6 Phoenix-ECO cells were plated per 10-cm

dish. The following day, cells were transfected by calcium phosphate transfection method with 10 μg of each plasmid and 5 μg of pCL-Eco retrovirus packaging plasmid. The media was changed 8 h after transfection. The viral supernatant was collected 48 h after transfection, passed through a 0.45 μm filter, pooled and used either fresh or snap-frozen.

For transduction, one volume of viral supernatant with polybrene (6 μg ml^{-1}) was added to mouse B cells after 24 h of activation with anti-CD40 plus IL-4, as previously described[9]. Plates were spun for 1.5 h at 2,400 r.p.m. and incubated overnight. Cells were washed and plated at a concentration of 5×10^5 cells per ml. On day 4 of stimulation, transduction efficiency was evaluated by measuring the percentage of transduced cells by enhanced green fluorescence protein expression (typical range was 50% to 85% of transduced cells). PI3K inhibitors were added at time of transduction and then maintained for the whole duration of the activation. CSR was evaluated by staining with Cy5-PE-labelled anti-mouse B220 (eBiosciences) and PE-labelled anti-mouse IgG_1 (BD Biosciences). Data acquisition was performed using a FACSVerse flow cytometer (BD biosciences). CSR ranged between 15% and 40% for retrovirus-transduced B cells. DNA was isolated from cells at day 4 of culture according to standard methods for HTGTS libraries.

CRISPR/Cas9 sgRNA design and cloning. For SpCas9 expression and generation of single guide RNA (sgRNA), the 20-nt target sequences were selected to precede a 5′-NGG protospacer-adjacent motif (PAM) sequence. The two *c-MYC*-targeting sgRNAs (1 and 2) and the *AICDA* sgRNA were designed with the CRISPR design tool from F. Zhang laboratory (http://crispr.mit.edu/). Oligonucleotides were purchased from Integrated DNA technology (IDT), annealed and cloned into the BsmbI-BsmBI sites downstream from the human U6 promoter in LentiCRISPR v2 plasmid (Addgene, 52961). Oligonucleotides used in this study for cloning are listed in Supplementary Table 7.

Lentiviral particles production. HEK293FT cells (Invitrogen) were maintained in 10% FBS-containing DMEM. To generate lentiviral particles, 5.5×10^6 HEK293FT cells were plated per 10 cm dish. The following day, cells were transfected by calcium phosphate transfection method with 7.2 μg of lentiCRISPR v2 plasmid, 3.6 μg of VSVG, 3.6 μg of RSV-REV, and 3.6 μg of PMDLg/pPRE. The media was changed 8 h after transfection. The viral supernatant was collected 36 h after transfection, passed through a 0.45 μm filter, pooled and used either fresh or snap-frozen.

Human cell lines transduction with CRISPR/Cas9 lentiviruses. For transduction of JeKo-1 and MEC1 with c-MYC CRISPR/Cas9 lentiviruses, a total number of 4×10^5 human neoplastic cells were plated into 6-well plates, at a concentration of 2×10^5 cells per ml. Lentiviral transduction was performed adding lentiviral supernatant, spinning for 1.5 h at 2,400 r.p.m. in the presence of polybrene (6 μg ml^{-1}). The viral supernatant was exchanged for fresh medium 8 h later. PI3K inhibitors were added 8 h before the infection and after washing. After 48 h, cells were selected with 0.2 μg ml^{-1} of puromycin to enrich for transduced cells. The cells were collected after 3 days from the puromycin addition. Genomic DNA was extracted as previously described for HTGTS libraries.

Generation of AID-knockout cell line clones. To generate the AID-knockout MEC-1 cell line, MEC-1 cells were transduced with AID CRISPR/Cas9 lentivirus according to the protocol described above. After 48 h from transduction cells were selected with 0.2 μg ml^{-1} of puromycin for 3 days. The selected cells were seeded as single colonies in 96-well plates by serial dilutions. After 3–4 weeks of culture, cells derived from each colony were used to assess AID-knockout by western blotting and genomic sequencing of the sgRNA target region.

Surveyor assay. The genomic region flanking the CRISPR target sites was PCR amplified (Surveyor primers are listed in Supplementary Table 7), and products were purified using PCR purification kit (QIAGEN) following the manufacturer's protocol. 400 ng total of the purified PCR products were mixed with 2 μl 10× Taq DNA Polymerase PCR buffer (Life Technologies) and ultra-pure water to a final volume of 20 μl, and subjected to a re-annealing process to enable heteroduplex formation: 95 °C for 10 min, 95 °C to 85 °C ramping at −2 °C per s, 85 °C to 25 °C at −0.25 °C per s, and 25 °C hold for 1 min. After re-annealing, products were treated with Surveyor nuclease and Surveyor enhancer S (Transgenomics) following the manufacturer's recommended protocol, and analysed on 2% high-resolution agarose gel (Sigma Aldrich). Gels were stained with ethidium bromide (Sigma Aldrich) and imaged with a Gel Doc gel imaging system (Bio-rad). Quantification was based on relative band intensities. Indel percentage was determined by the formula, $100 \times (1-(1-(b+c)/(a+b+c))\,1/2)$, where a is the integrated intensity of the undigested PCR product, and b and c are the integrated intensities of each cleavage products.

Generation of HTGTS libraries. DNA was prepared from mouse and human B cells at day 4 of culture using rapid lysis buffer containing 10 μg ml^{-1} Proteinase K and incubation at 56 °C overnight, followed by standard isopropanol extraction, wash in ethanol 70% and resuspension in TE buffer. HTGTS libraries were generated by emulsion-mediated PCR (EM–PCR) methods as previously described[9]. In brief, genomic DNA was digested overnight with HaeIII frequent cutter enzyme. HaeIII-generated blunt ends were A-tailed with Klenow polymerase (3′–5′ exo-; New England Biolabs). An asymmetric adaptor (composed of an upper linker and a lower 3′-modified linker) was then ligated to fragmented DNA. To remove the unrearranged I-SceI cassettes or the unrearranged endogenous *c-myc* locus, ligation reactions were digested with both EcoRV and XbaI. In the first round of PCR, DNA was amplified using a biotinylated forward primer and an adaptor-specific reverse primer and Phusion polymerase (Thermo-Scientific). 20 PCR cycles were performed in the following conditions: 98 °C for 10 s, 58 °C for 30 s, and 72 °C for 30 s. Multiple reactions were performed in generating large-scale libraries. Biotinylated PCR products were isolated using the Dynabeads MyOne Streptavidin C1 kit (Invitrogen), followed by an additional 2-h-digestion with blocking enzymes was performed. PCR products were eluted from the beads by 30 min incubation at 65 °C in 95% formamide/10 mM EDTA and purified. The purified products were then amplified in a second round with em-PCR in an oil-surfactant mixture. The emulsion mixture was divided into individual aliquots and PCR was performed using the following conditions: 20 cycles of 94 °C for 30 s, 60 °C for 30 s, and 72 °C for 1 min. Following PCR, the products were pooled and centrifuged in a table-top centrifuge for 5 min at 14,000 r.p.m. to separate the phases and the oil layer was removed. The sample was then extracted three times with diethyl ether and DNA was re-purified. The third, non-emulsion, round of PCR (10 cycles) was performed with the same primers as in round 2, but with the addition of linkers and barcodes for Illumina Mi-seq sequencing. PCR products were size-fractionated for DNA fragments between 300 and 800 base pairs on a 1% agarose gel, column purified (QIAGEN) before loading onto Illumina Mi-seq machine for sequencing.

Nucleotide sequences of junctions were generated by Mi-seq (Illumina NS500 SE150) sequencing at the Molecular Biology Core Facilities of the Dana-Farber Cancer Institute. At least three independent libraries were generated and analysed for each experimental condition (Supplementary Table 1). Oligonucleotide primers used for mouse and human libraries preparation are listed in Supplementary Table 7.

HTGTS data processing. First, we applied prinseq 0.2 (ref. 35) to remove sequences with exact PCR duplicates, mean quality score <20 and length <50. Next, reads for each experimental condition were demultiplexed by designed barcode, and then filtered by the presence of the primer plus additional 5 downstream bases as bait portion. Barcodes and primers used are listed in Supplementary Tables 1, 7. Lastly, the barcode, primer and bait portion of the remained sequences were masked for alignment analysis.

Alignment and filtering. The sequences for each experiment were aligned and filtered as previously described[9]. Briefly, we aligned sequences to the mouse reference genome (GRCm37/mm9) or human genome (GRCh38/hg38) using BLAT, and then filtered artificial junctions by removing PCR repeats (reads with same junction position in alignment to the reference genome and a start position in the read less than 3 bp apart), invalid alignments (including alignment scores <30, reads with multiple alignments having a score difference <4 and alignments having 10-nucleotide gaps) and ligation artefacts (for example, random HaeIII restriction sites ligated to bait breaksite). Translocation junction position was determined on the basis of the genomic position of the 5′ end of the aligned read.

Hotspot identification. Translocation junctions data from similar size biological replicates were pooled for hotspots identification. First, we employed SICER 1.1 (ref. 36) to identify candidate regions where HTGTS junctions were significantly enriched against genome-wide background. The parameters used were as follows: window size, 1,000; gap size, 2,000; *e*-value, 0.000001; redundancy, 1; effective genome fraction, 0.77 for mouse or 0.74 for human. Next, we eliminated from analysis the following hotspots: (1) hotspots in the region ± 4 Mb around Myc bait breaksite including the *Pvt1* gene as previously described[9]; (2) hotspots with junctions number less than 5; (3) hotspots with strand bias. We used the following entropy formula to measure strand bias as $S = -P \times \log_2(P) - (1-P) \times \log_2(1-P)$, where P is the percentage of junctions from the plus stand, and $1-P$ is the percentage of junctions from the minus strand. If P or $1-P$ were <10% (entropy $S < 0.47$), we eliminated the hotspot for a strand bias; (4) hotspots without significant enrichment against the local background. The local background P value was calculated by Poisson distribution against the region that surrounds the hotspot (± 3 times the size of the hotspot). Bonferroni correction was used to adjust P value for multiple tests. We set adjusted $P = 0.01$ as significance level. For JeKo-1, owing to its complex karyotype[37], which increases the local noise level, we set more stringent criteria for hotspot identification, including adjust $P < 0.00001$ and region size <30 kb. Hotspots from different experiments that partially overlapped were merged to define common hotspot regions that were used as reference to compare junction frequency between different experiments.

Junction frequency calculation and representation. Translocation junction frequencies in hotspots were normalized to reads per million (RPM). In box plot for fold-change comparison, to avoid 'division by zero' error, 0 was replaced with 1, and then normalized to corresponding RPM in library. For clustering heat map, the RPM was transformed into a $\log_2$ value, and then median centred. The genome-wide translocation circle plots were made using Circos tool[38]. Translocation junction distributions were visualized by IGV 2.3.6 (ref. 39). For translocation frequency distribution around ConvT or SE centres, centres were defined as the central bp position of the ConvT or SE region, as we previously defined[10]. Regions ± 4 Mb around the I-SceI c-myc breaksite on chromosome 15 and the IgH S regions on chromosome 12 were excluded in the analysis of junctions around TSS, ConvT or SE centres. For SE analysis, hotspots embedded within two adjacent SEs with centre-to-centre distance <100 kb were excluded because it was not possible to univocally assign them with one of the two SEs. All ChIP–seq data used in this study were obtained from previously published data including SE[10], AID[17], Spt5 and Pol II[20].

Statistical comparison of junction frequency in hotspots. Statistical significance of differential junction frequency in hotspots were performed using SICER 1.1 (ref. 36) with the following parameters: window size, 1,000; gap size, 2,000; *e*-value, 0.000001; effective genome fraction, 0.77 (mouse) or 0.74 (human); and FDR = 0.01 or FDR = 0.1.

GRO-seq assay and analysis. Nuclei were isolated at day 2 from B cells activated with anti-CD40 plus IL-4 and treated with PI3K inhibitors, as previously described[9]. GRO-seq libraries were sequenced on the Hi-seq 2,000 platform with single-end reads and analysed as follows: GRO-seq data were aligned using Bowtie software[40] mouse reference genome (GRCm37/mm9). Uniquely mapped, non-redundant sequence reads were retained. Next, we used HOMER software to count reads and calculate the nascent RNA expression levels as RPKM (reads per 1,000 bp per million mapped reads) in whole genes or in focal translocation clusters, and to identify transcripts from both strands of chromosomes[41]. The ConvT region was defined as sense and antisense transcription overlaps that were longer than 100 bp[10]. Statistical analysis for differential expression and log fold-change calculation were performed using DESeq2 (ref. 42) in whole genes or in focal translocation clusters. The MA-plot of log fold-changes against mean of normalized counts were generated by function plotMA in R package DESeq2 (ref. 42).

Amplification and targeted re-sequencing. Phusion High Fidelity DNA polymerase (Thermo-Scientific) was used to amplify selected regions from template genomic DNA. Oligonucleotide primers are listed in Supplementary Table 7: amplification conditions for each gene are available on request. Amplification products were purified using PCR purification kit (QIAGEN) and GEL extraction kit (QIAGEN) following the manufacturer's protocol and sequenced bi-directionally in a Mi-seq (Illumina NS500) sequencing platform at the Molecular Biology Core Facilities of the Dana-Farber Cancer Institute.

SHM data analysis. For SHM calculations, mouse and human intragenic and intergenic regions were targeted re-sequenced with primers indicated in Supplementary Table 7. Sequences with mean quality score <20 and length <50 were removed. Samples with less than 100 reads were excluded from analysis. The remained sequences were used to calculate mutation rate. Sequences obtained from each designed region were aligned to the reference sequence using BLASTN with alignment length >200. Mutations were calculated after filtering steps, as previously described[43]. Briefly, mutations first had to pass a Neighbourhood Quality Standard criteria requiring a minimum Phred score of 30 for the mutation itself, and 20 for the five adjacent bases on either side. Mutations that were within five bases of more than two additional mutations were excluded. Mutations within two bases of a deletion or insertion were also excluded. In addition, bases with mutation rate >0.01 were excluded as a result of overwhelming influence of sequence error or SNP, of which bases with mutation rate >0.2 were further regarded as SNP and were excluded. Finally, the average base mutation rate of 1–200 bp passing the above criteria were calculated from forward sequence, as well as reverse sequences if applicable. For average base mutation rates of C-to-T or G-to-A transitions, only C or G bp sites we counted. Mutations on the VB1-8 productive allele were performed and analysed as recently described[19].

Code availability. Source code for genomic event analysis tools (GEAT) developed in our laboratory to perform the analysis is available at https://github.com/geatools/geat.

Data availability. All sequencing data has been deposited in the Gene Expression Omnibus database under accession number GSE77788. Source Data for figures are provided with the online version of the paper.

31. Muramatsu, M. *et al.* Class switch recombination and hypermutation require activation-induced cytidine deaminase (AID), a potential RNA editing enzyme. *Cell* **102,** 553–563 (2000).
32. Cato, M. H., Yau, I. W. & Rickert, R. C. Magnetic-based purification of ntouched mouse germinal center B cells for *ex vivo* manipulation and biochemical analysis. *Nat. Protocols* **6,** 953–960 (2011).
33. Kovalchuk, A. L., Müller, J. R. & Janz, S. Deletional remodeling of c-myc-deregulating chromosomal translocations. *Oncogene* **15,** 2369–2377 (1997).
34. Ramiro, A. R. *et al.* AID is required for *c-myc*/IgH chromosome translocations *in vivo*. *Cell* **118,** 431–438 (2004).
35. Schmieder, R. & Edwards, R. Quality control and preprocessing of metagenomic datasets. *Bioinformatics* **27,** 863–864 (2011).
36. Zang, C. *et al.* A clustering approach for identification of enriched domains from histone modification ChIP–seq data. *Bioinformatics* **25,** 1952–1958 (2009).
37. Camps, J. *et al.* Genomic imbalances and patterns of karyotypic variability in mantle-cell lymphoma cell lines. *Leuk. Res.* **30,** 923–934 (2006).
38. Krzywinski, M. *et al.* Circos: an information aesthetic for comparative genomics. *Genome Res.* **19,** 1639–1645 (2009).
39. Robinson, J. T. *et al.* Integrative genomics viewer. *Nat. Biotechnol.* **29,** 24–26 (2011).
40. Langmead, B. & Salzberg, S. L. Fast gapped-read alignment with Bowtie 2. *Nat. Methods* **9,** 357–359 (2012).
41. Heinz, S. *et al.* Simple combinations of lineage-determining transcription factors prime *cis*-regulatory elements required for macrophage and B cell identities. *Mol. Cell* **38,** 576–589 (2010).
42. Love, M. I., Huber, W. & Anders, S. Moderated estimation of fold change and dispersion for RNA-seq data with DESeq2. *Genome Biol.* **15,** 550 (2014).
43. Liu, M. *et al.* Two levels of protection for the B cell genome during somatic hypermutation. *Nature* **451,** 841–845 (2008).

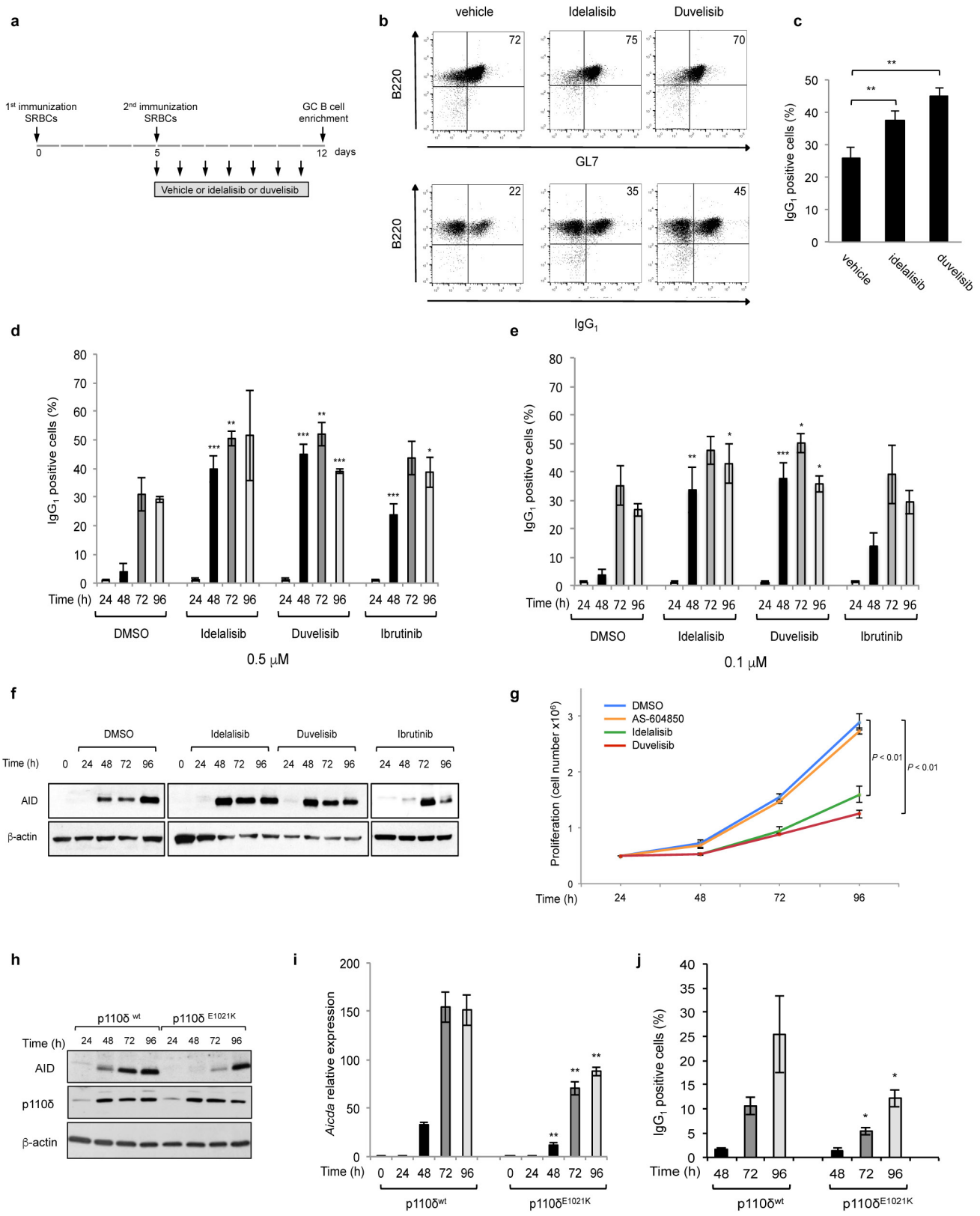

Extended Data Figure 1 | See next page for caption.

Extended Data Figure 1 | PI3Kδ blockade increases AID expression and CSR in activated mouse B cells. a, Schematic representation of the *in vivo* experiment in wild-type mice immunized with sheep red blood cells and treated with the indicated inhibitors ($n = 6$ biological replicates). **b**, Representative dot plots of IgG_1 switched $GL7^+$ $B220^+$ germinal centre B cells from mice treated with vehicle or the PI3Kδ inhibitors. **c**, Mean IgG_1 CSR analysed by flow cytometry in control and idelalisib- or duvelisib-treated mice. **d**, **e**, IgG_1 CSR analysed by flow cytometry in activated B cells treated with 0.5 μM (**d**) or 0.1 μM (**e**) of the indicated drugs. **f**, Western blot for AID protein expression in activated B cells treated with the indicated inhibitors (0.1 μM) ($n = 3$ biological replicates). For gel source data, see Supplementary Fig. 1. **g**, Viable cells were counted at the indicated time points by Trypan Blue exclusion in activated B cells treated with the indicated inhibitors (1 μM). **h**, Representative western blot for AID and PI3K p110δ protein expression in mouse B cells transduced with retrovirus expressing PI3K $p110\delta^{WT}$ or the p110δ(E1021K) active mutant ($n = 4$ biological replicates). **i**, *Aicda* mRNA levels analysed by qRT–PCR in activated B cells transduced with PI3K $p110\delta^{WT}$ or the p110δ(E1021K) active mutant. *P* values calculated by two-tailed Student's *t*-test by comparing PI3K p110δ(E1021K) versus PI3K $p110\delta^{WT}$ cells. **j**, IgG_1 CSR analysed by flow cytometry in activated B cells expressing PI3K $p110\delta^{WT}$ or the p110δ(E1021K) active mutant. Data are expressed as mean ± s.d. ($n = 3$); $^*P < 0.05$, $^{**}P \leq 0.01$, $^{***}P \leq 0.001$, two-tailed Student's *t*-test (**c**–**e**, **g**, **i**, **j**).

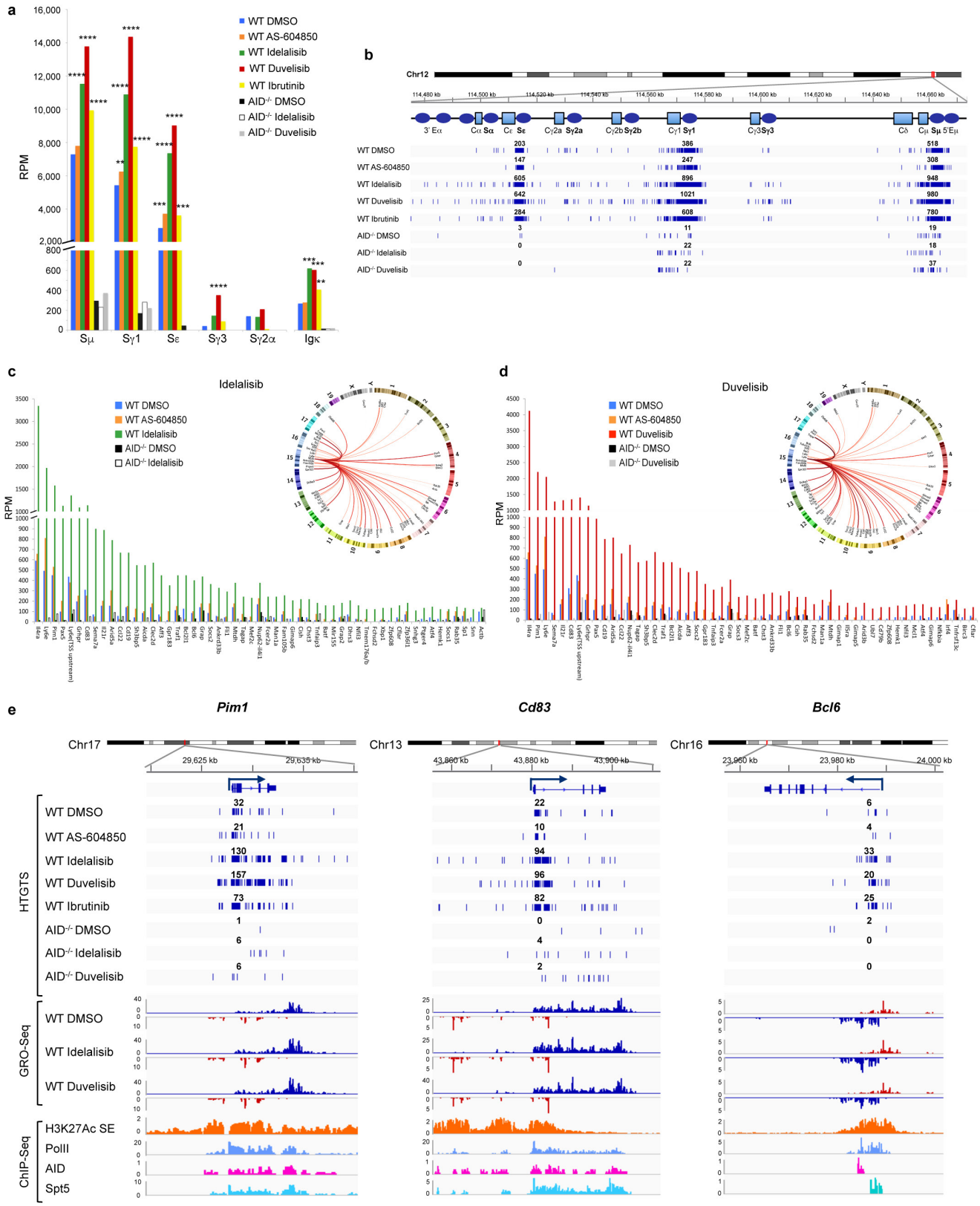

Extended Data Figure 2 | See next page for caption.

Extended Data Figure 2 | Frequency of AID-mediated translocation junctions in activated mouse B cells is increased by PI3Kδ blockade. **a**, Frequency of chromosomal translocations between the *c-myc* and the *Igh* and *Igk* loci, represented as reads per million (RPM) in wild-type and *Aicda*$^{-/-}$ activated B cells treated with the indicated inhibitors. Significance is calculated as FDR by comparing AS-604850, idelalisib or duvelisib to DMSO-treated B cells as indicated in the Methods. **FDR $\leq$ 0.01, ***FDR $\leq$ 0.001, ****FDR $\leq 1 \times 10^{-10}$. **b**, Detailed view of the distribution of translocation junctions in the *Igh* locus from wild-type and *Aicda*$^{-/-}$ mouse B cells treated with the indicated inhibitors. Numbers of translocation junctions in focal clusters are indicated in bold. **c**, Histograms showing the AID off-targets with significantly increased frequency of HTGTS junctions (FDR $<$ 0.001) induced by idelalisib treatment as compared to DMSO (54 out of 59 off-target sites, 91.5%) in wild-type and *Aicda*$^{-/-}$ activated B cells. Significance is calculated as indicated in the Methods. Circos plots show the overview of genome-wide translocation distribution. Individual translocations from *c-myc* to AID target sites are represented as arcs originating from *c-myc* DSB breaks on chromosome 15. Thickness and red colour intensity of the arcs represent the fold increase of translocation frequency in idelalisib versus DMSO-treated cells. **d**, Histograms showing the AID off-targets with significantly increased frequency of translocation junctions (FDR $<$ 0.001) induced by duvelisib treatment as compared to DMSO (55 out of 63 off-target sites, 87.3%) in wild-type and *Aicda*$^{-/-}$ activated B cells. Significance is calculated as indicated in the Methods. Circos plots show the overview of genome-wide translocation distribution. **e**, Translocation junction distribution (top), GRO-seq (middle) and ChIP–seq (bottom) profiles in three representative AID off-target genes (*Pim1*, *Cd83*, *Bcl6*) in wild-type and *Aicda*$^{-/-}$ activated B cells treated with idelalisib, duvelisib or ibrutinib. GRO-seq sense and antisense transcription is displayed in blue and red profiles. Numbers of translocation junctions in focal clusters are indicated in bold.

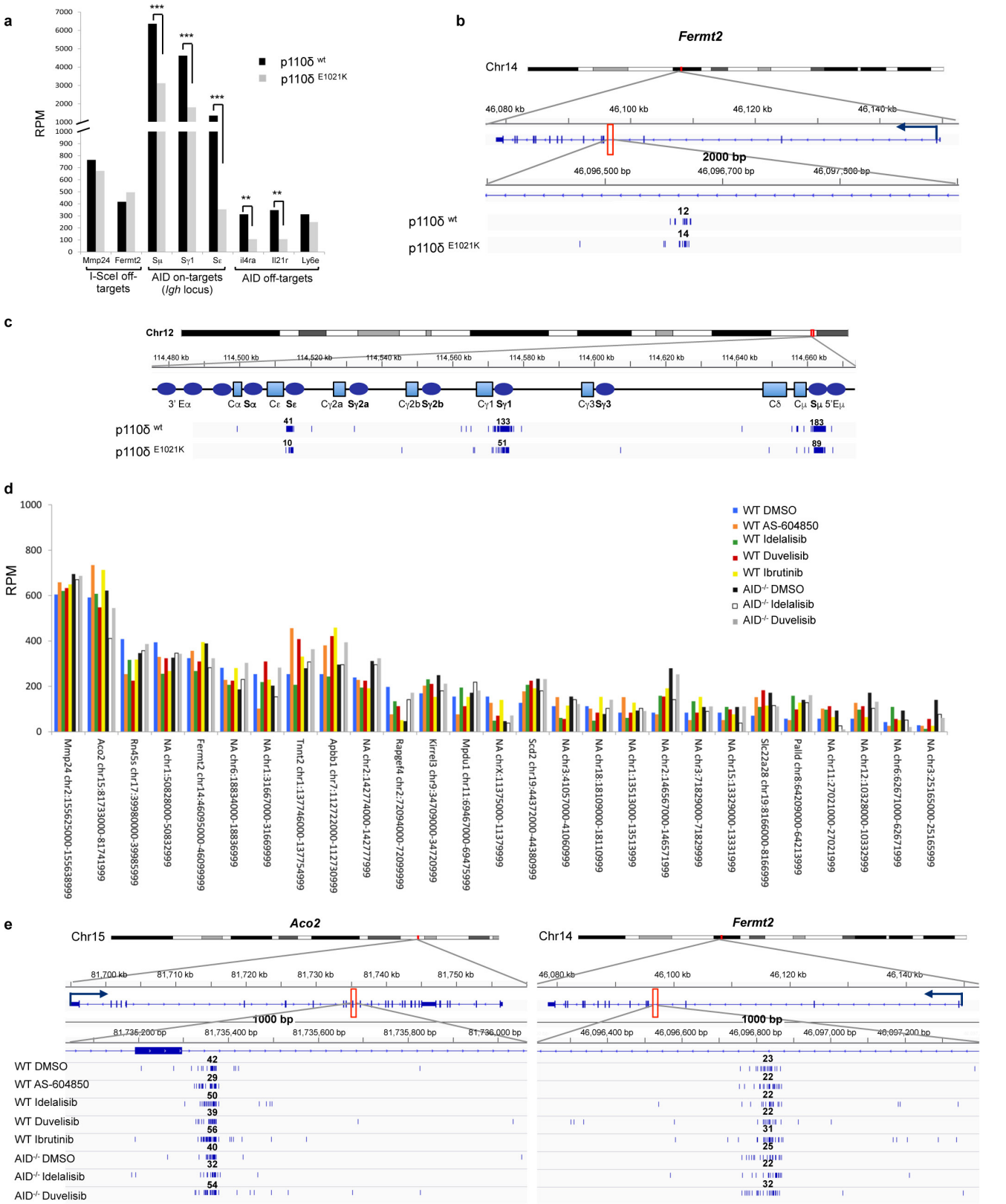

Extended Data Figure 3 | Frequency of AID on-target and off-target translocation junctions is reduced in activated mouse B cells transduced with the PI3K p110δ(E1021K) active mutant. a, Histograms showing junction frequency in activated mouse B cells transduced with retrovirus expressing PI3K p110δ^{WT} or the p110δ(E1021K) active mutant. Significance is calculated as FDR by comparing PI3K p110δ^{WT} to p110δ(E1021K)-transduced B cells as indicated in the Methods. **FDR ≤ 0.01, ***FDR ≤ 0.001. **b** Detailed view of the distribution of translocation junctions in one representative I-SceI off-target (*Fermt2*). **c**, Detailed view of the distribution of translocation junctions in the *Igh* locus. Numbers of translocation junctions in focal clusters are indicated in bold. **d**, Histograms showing frequency of translocation junctions as RPM for I-SceI off-targets in wild-type and *Aicda*$^{-/-}$ activated B cells treated with the indicated inhibitors. **e**, Detailed view of the distribution of translocation junctions in two representative I-SceI off-target sites (*Aco2* and *Fermt2*). Numbers of translocation junctions in focal clusters are indicated in bold.

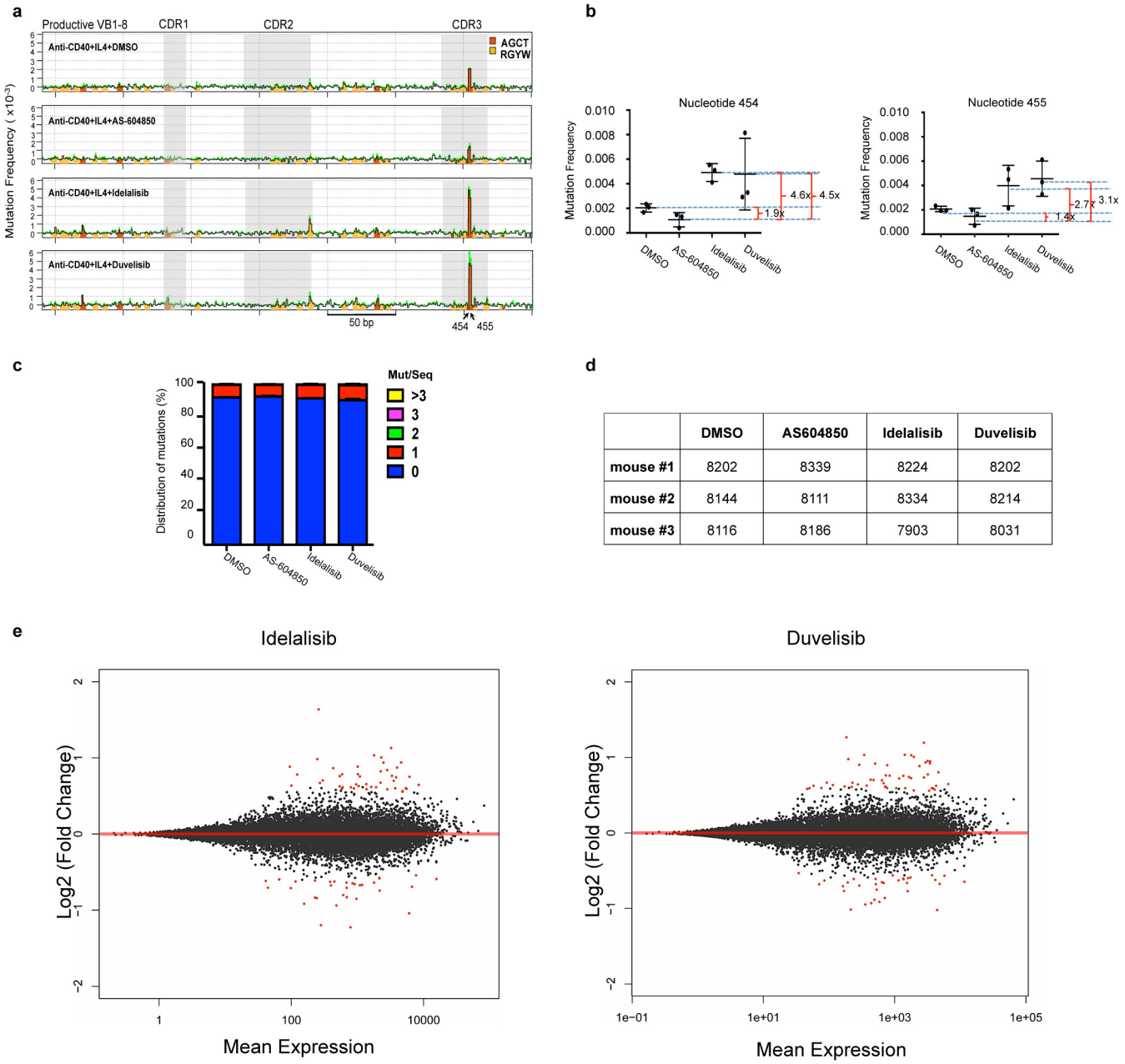

	DMSO	AS604850	Idelalisib	Duvelisib
mouse #1	8202	8339	8224	8202
mouse #2	8144	8111	8334	8214
mouse #3	8116	8186	7903	8031

Extended Data Figure 4 | PI3Kδ blockade increases SHM frequency in *Igh* V region in activated mouse B cells and transcription of genes. **a**, Map of mutations on the VB1-8 productive allele sequence in activated B cells treated with the indicated inhibitors. The *y* axis indicates the mutation frequency at each nucleotide in sequences that have 0 to 2 mutations per sequence at day 4 of stimulation after subtraction of mutation frequency at day 0 of stimulation. Green shading indicates top s.e.m. from three independent mice. Orange and yellow bars mark the positions of AGCT and other RGYW motif that is not AGCT, respectively. One experiment is represented out of three biological replicates with similar results. **b**, Mutation frequency of nucleotide 454 (top) and 455 (bottom) of the VB1-8 productive allele at day 4 after subtraction of mutation frequency at day 0. Data represent mean of three independent stimulations of B cells from three independent mice. Error bars indicate s.d. Fold changes between each mean are indicated. **c**, Stacking bar chart shows percentage of sequences that have the indicated number of mutations per sequence. Data are displayed as the mean from three independent stimulations of B cells derived from three mice. Error bars indicate s.e.m. **d**, The number of reads from individual mice for the data are shown in **a**. **e**, MA plots of log fold changes generated by DESeq2 in R package against mean expression (normalized counts) from GRO-seq data for idelalisib or duvelisib over DMSO. Red dots indicate significantly upregulated genes ($n = 39$ idelalisib, $n = 47$ duvelisib) or downregulated genes ($n = 32$ idelalisib, $n = 33$ duvelisib) with multiple test adjusted P value < 0.1 (Supplementary Table 3).

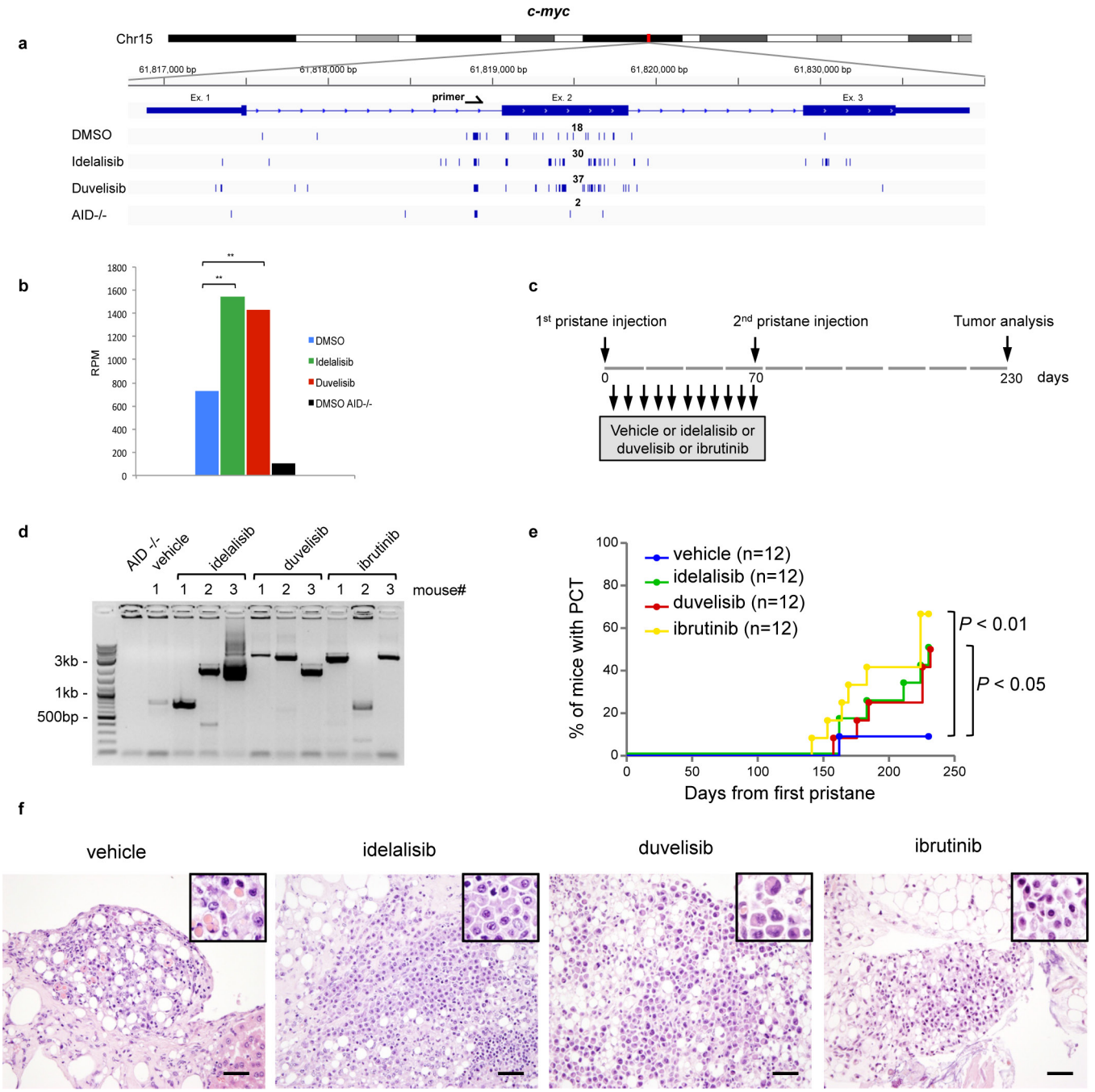

Extended Data Figure 5 | PI3Kδ inhibitors and ibrutinib increase *c-myc* DSB formation and the incidence of plasma cell tumour in mice. a, Detailed view of the distribution of rearrangements (deletions or inversions) in the *c-myc* locus in mice treated as above. Numbers of translocation junctions in focal clusters are indicated in bold. **b**, RPM frequency of rearrangements (deletions or inversions) in the *c-myc* locus in germinal centre B cell from mice treated *in vivo* with the idelalisib or duvelisib. Junctions within ± 300 bp of primer region were excluded. Significance is calculated as FDR by comparing idelalisib or duvelisib to DMSO-treated mouse as indicated in the Methods. **FDR ≤ 0.01. **c**, Schematic representation of the experimental outline of pristane-induced plasma cell tumours in mice treated with PI3Kδ inhibitors and ibrutinib. The mice were treated in two independent biological experimental replicates, each consisting of 6 mice per group. **d**, Direct PCR assay for *Igh–c-myc* translocation in mice with plasma cell tumours. Translocations from c-myc to the IgHα locus are shown. Translocations for the only mouse in the vehicle group and from three example mice from treated groups are shown. Bands were purified from gels and were sequenced to confirm the *Igh–c-myc* translocation junction. For gel source data, see Supplementary Fig. 1. **e**, Development of plasma cell tumour in mice induced with pristane and treated with idelalisib, duvelisib or ibrutinib is plotted over time. The presence of plasma cell tumours was confirmed by histology ($n = 12$ for each treatment in 2 independent cohorts of 6 mice). *P* values calculated by log-rank (Mantel–Cox) test. **f**, Example histology of plasma cell tumours in mice induced with pristane and treated with the indicated drugs. Magnification, 40×; scale bar, 50 μm; insets: high magnification image of clusters of atypical plasma cells.

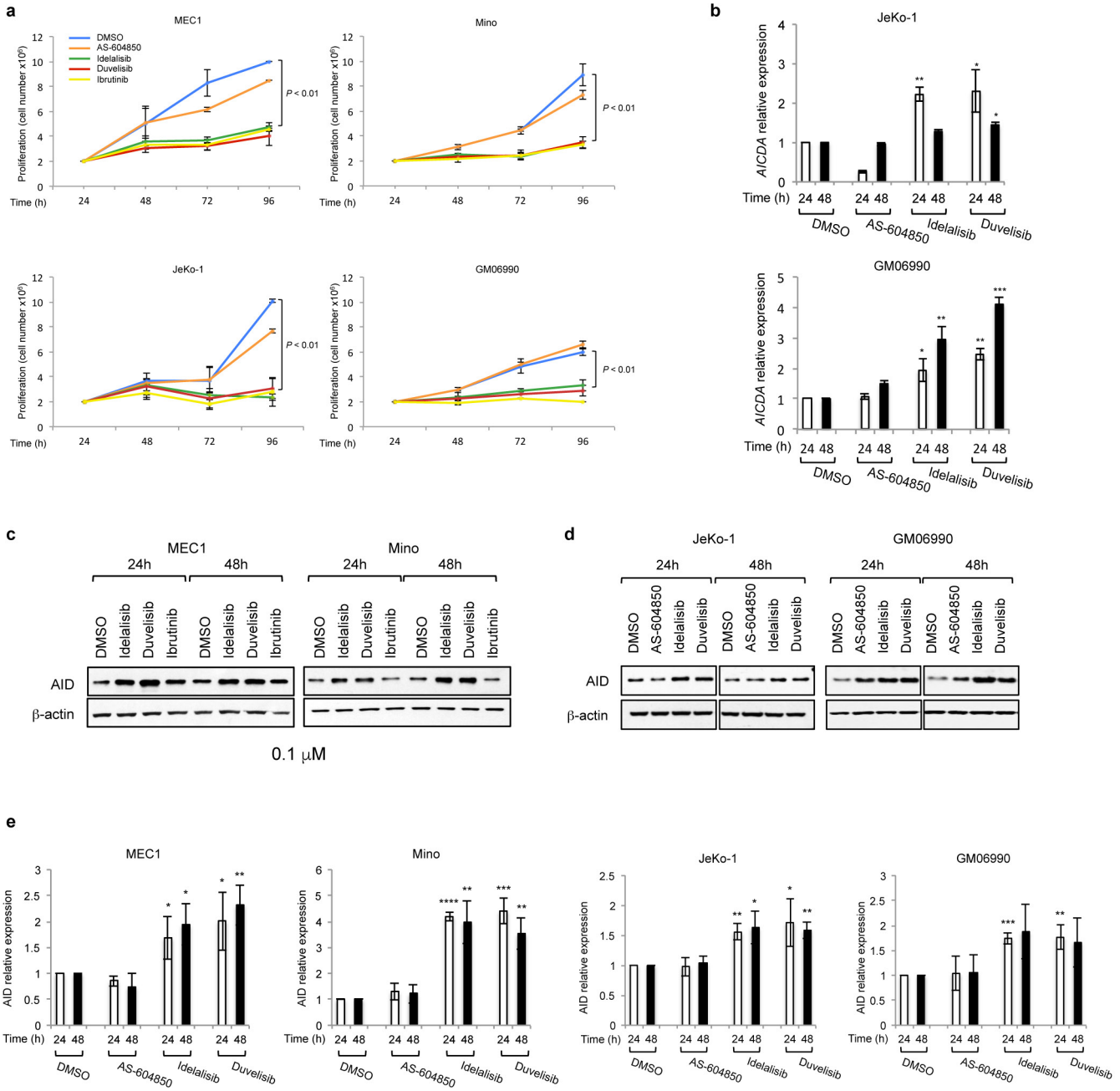

Extended Data Figure 6 | PI3Kδ blockade increases AID expression in human B-cell lines. a, Viable cells were counted at the indicated time points by Trypan Blue exclusion in MEC1, Mino, JeKo-1 and GM06990 cell lines treated with the indicated inhibitors (1 μM). **b**, Histograms showing the *AICDA* mRNA relative expression in JeKo-1 and GM06990 cell lines treated with 1 μM inhibitors. **c**, Western blot for AID protein expression in MEC1 and Mino B-cell lines treated with 0.1 μM inhibitors ($n = 2$ biological replicates). **d**, Western blot for AID protein expression in JeKo-1 and GM06990 B-cell lines treated with 1 μM inhibitors ($n = 4$ biological replicates). For gel source data, see Supplementary Fig. 1. **e**, Histograms showing the AID protein relative expression at the indicated time points in MEC1, Mino, JeKo-1 and GM06990 cell lines treated with 1 μM inhibitors. AID abundance was measured by ImageJ software and normalized for the β-actin intensity of the corresponding lane. Data are expressed as mean ± s.d. ($n = 3$ biological replicates). $^{*}P < 0.05$, $^{**}P \leq 0.01$, $^{***}P \leq 0.001$, $^{****}P \leq 0.0001$, two-tailed Student's *t*-test (**a**, **b**, **e**).

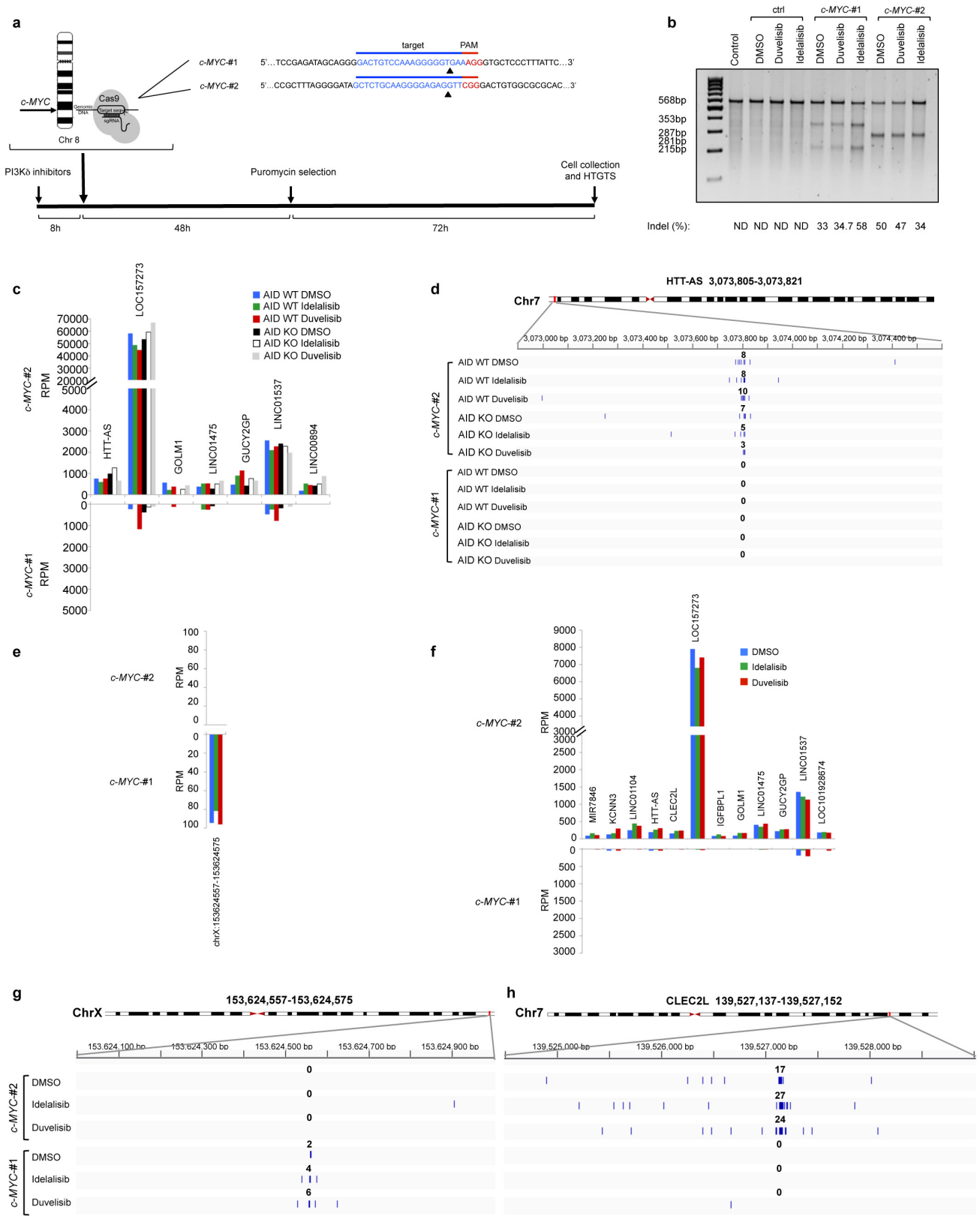

Extended Data Figure 7 | See next page for caption.

Extended Data Figure 7 | Strategy to generate chromosomal translocations in human B cells from DSBs introduced in the *c-MYC* locus by CRISPR/Cas9 technology. a, Schematic representation of the experimental strategy employed to generate chromosomal translocation from the *c-MYC* locus by introducing DSBs in *c-MYC* intron 1 by two different sgRNAs (*c-MYC*-#1 or *c-MYC*-#2). Arrowheads (black) indicate the cleavage sites introduced by Cas9 and PAM sequence is in red. **b**, Surveyor Assay to measure the cutting efficiency of the *c-MYC* gene targeted in JeKo-1 cell line. Locus modification efficiencies are analysed 5 days after transduction of *c-MYC*-#1 or *c-MYC*-#2 Cas9 lentivirus. Estimated indel formation is indicated below each target. Black arrowheads indicate the size of the observed bands. N.D.:, not detectable. One representative experiment out of three performed with comparable results is shown. For gel source data, see Supplementary Fig. 1. **c**, Histograms showing frequency of translocation junctions in Cas9 off-target sites for *c-MYC*-#2 sgRNAs in MEC1 cell line treated with idelalisib or duvelisib. AID-knockout MEC1 cells were generated by CRISPR/Cas9-mediated deletion (Extended Data Fig. 8e). For each treatment, data are from pooled HTGTS libraries of similar size from independent experiments as indicated in Supplementary Table 1. **d**, Detailed view of the distribution of translocation junctions in representative Cas9 off-target site for *c-MYC*-#2. Numbers of translocation junctions in focal clusters are indicated in bold. **e**, **f**, Histograms showing translocation junctions frequency in Cas9 off-targets sites for c-*MYC*-#1 (**e**) or c-*MYC*-#2 (**f**) sgRNAs in JeKo-1 cell line treated with idelalisib or duvelisib. For each treatment, data are from pooled HTGTS libraries of similar size as indicated in Supplementary Table 1. **g**, **h**, Detailed view of the distribution of translocation junctions in representative Cas9 off-target sites for c-*MYC*-#1 (**g**) or c-*MYC*-#2 (**h**). Numbers of translocation junctions in focal clusters are indicated in bold.

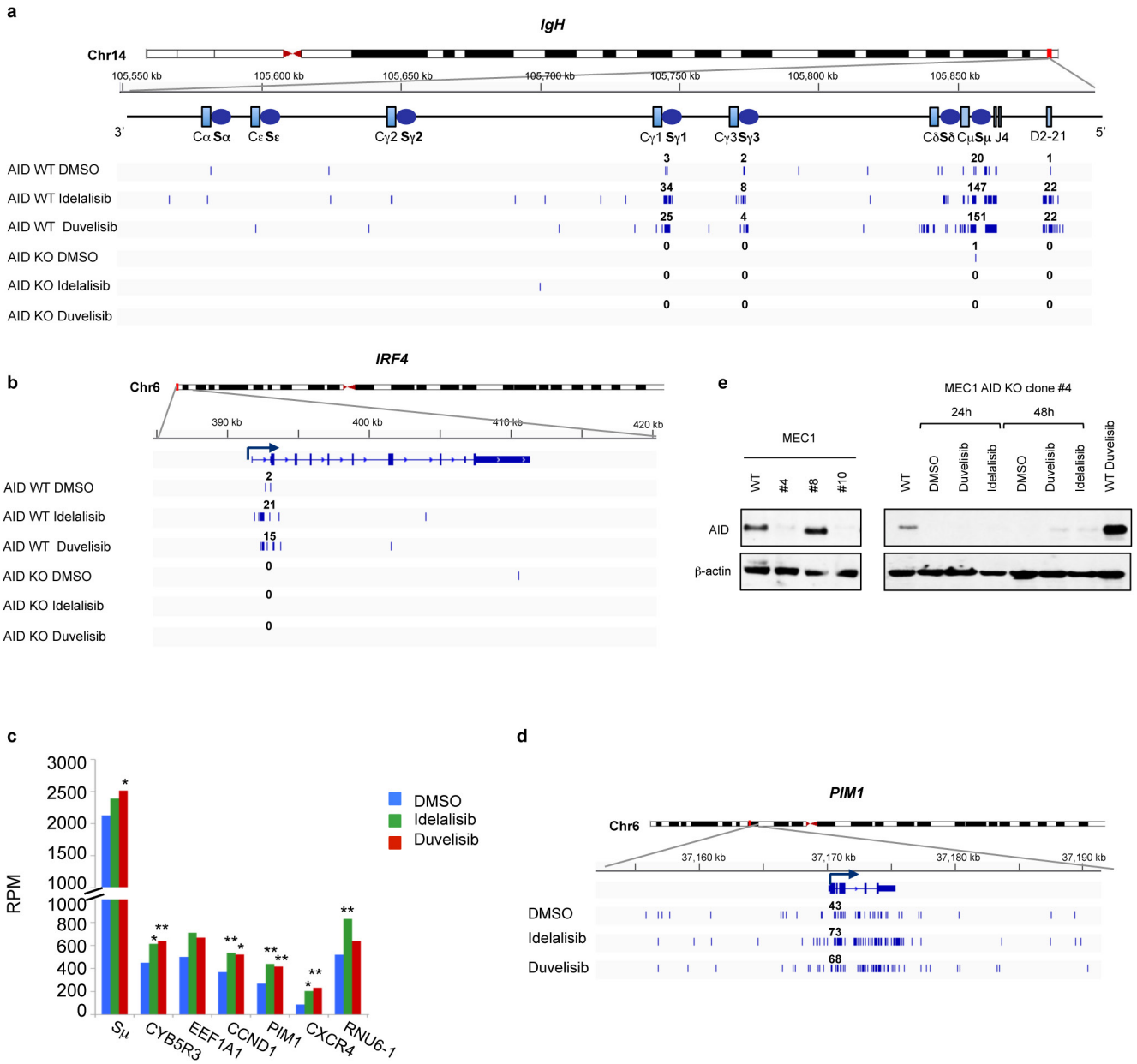

Extended Data Figure 8 | Translocations to AID off-targets are increased by idelalisib and duvelisib treatment in MEC1 and JeKo-1 cell line. a, **b**, Distribution of translocation junctions in the *IGH* locus (**a**) and in the *IRF4* AID off-target gene (**b**) in MEC1 cells. AID-knockout MEC1 cells were generated by CRISPR/Cas9-mediated deletion. Numbers of translocation junctions in focal clusters are indicated in bold. **c**, Translocation junction frequency in AID on-target and AID off-target sites in JeKo-1 B-cell line treated with DMSO, idelalisib or duvelisib (1 μM). Data are from pooled HTGTS libraries of similar size (Supplementary Tables 1, 4) from 3 independent experiments. Statistical analysis in Methods. *FDR ≤ 0.1, **FDR ≤ 0.01. **d**, Distribution of translocation junctions in the *PIM1* AID off-target gene in JeKo-1 B-cell line. Numbers of translocation junctions in focal clusters are indicated in bold. **e**, AID-knockout MEC1 cells were generated by CRISPR/Cas9-mediated deletion, cloned and validated by indel sequencing of the Cas9 target site and by AID protein expression. Western blot for AID showing the parental cells (wild type), two AID-knockout clones (4 and 10) and one AID wild-type clone (6). AID-knockout clone 4 was treated with 1 μM DMSO, idelalisib or duvelisib (right panel) ($n = 2$ biological replicates). For gel source data, see Supplementary Fig. 1.

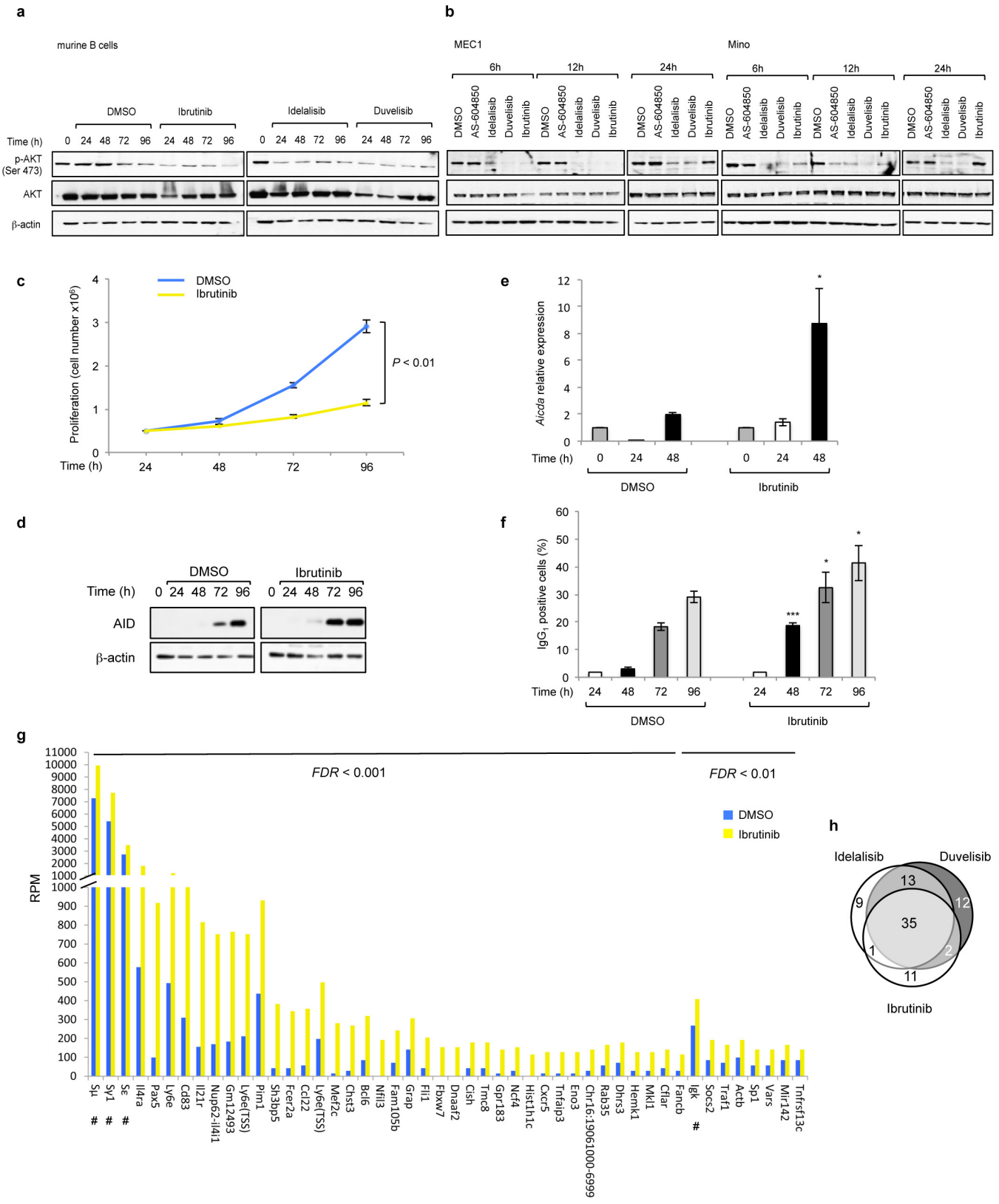

Extended Data Figure 9 | See next page for caption.

Extended Data Figure 9 | Ibrutinib increases AID expression and the frequency of translocations to AID on- and off-target sites in mouse activated B cells. a, AKT phosphorylation was detected by western blot in mouse activated B cells treated with DMSO, idelalisib, duvelisib or ibrutinib (1 μM) for the indicated time points ($n = 2$ biological replicates). For gel source data, see Supplementary Fig. 1. **b**, MEC1 and Mino human lymphoma cells were treated with the indicated inhibitors (1 μM) and AKT phosphorylation was evaluated by western blot ($n = 3$ biological replicates). **c**, Viable cells were counted at the indicated time points by Trypan Blue exclusion in activated B cells treated with DMSO or ibrutinib (1 μM). Data are expressed as mean ± s.d. ($n = 3$). *P* values calculated by two-tailed Student's *t*-test. **d**, Western blot for AID protein expression in activated B cells treated with 1 μM ibrutinib. The DMSO panel from Fig. 1a is shown for comparison ($n = 3$ biological replicates). **e**, *Aicda* mRNA levels analysed by qRT–PCR in activated B cells treated with DMSO or ibrutinib (1 μM). **f**, IgG_1 CSR in activated B cells analysed by flow cytometry. Data are expressed as mean ± s.d. ($n = 3$ biological replicates). $^*P < 0.05$, $^{***}P \leq 0.001$, two-tailed Student's *t*-test (**e**, **f**). **g**, Histograms showing translocation junction frequency to AID on-target (#, *Igh* and *Igk* loci) and off-target sites in activated B cells treated with ibrutinib. Targets are divided on the basis of the statistical significance of increased junctions frequency compared to DMSO treatment (FDR < 0.001 on the left; FDR < 0.01 on the right). Statistical analysis is indicated in the Method. For each treatment, data are from pooled HTGTS libraries of similar size from independent experiments as indicated in Supplementary Tables 1, 5. **h**, Venn diagrams showing the fraction of AID off-target sites shared in activated mouse B cells treated with ibrutinib, idelalisib or duvelisib.

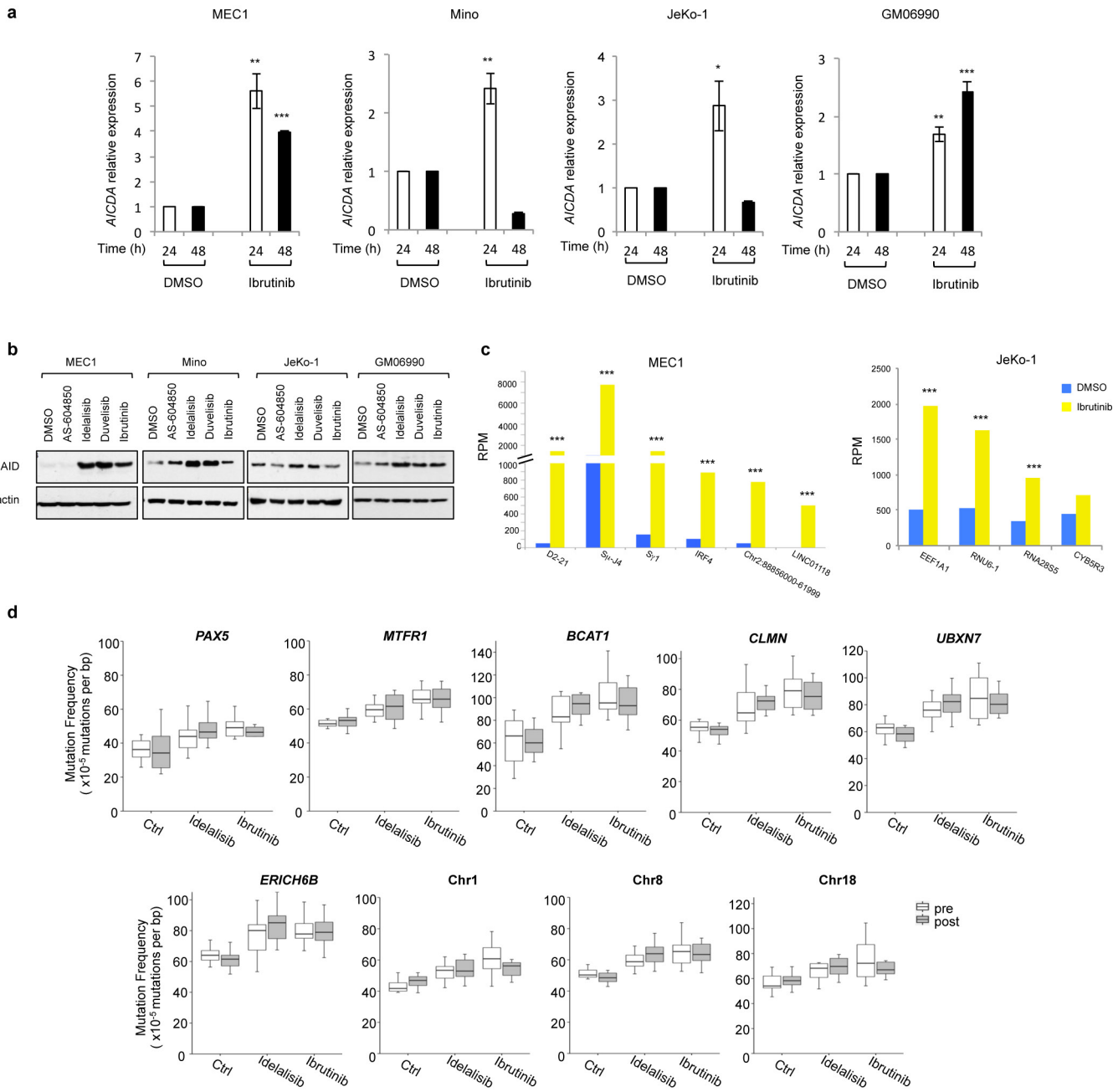

Extended Data Figure 10 | Ibrutinib increases AID expression and the frequency of translocations to AID on- and off-target sites in human B cells. a, *AICDA* mRNA levels analysed by RT–qPCR in MEC1, Mino, JeKo-1 and GM06990 cell lines after treatment with DMSO or ibrutinib. Data are expressed as mean ± s.d. ($n = 3$ technical replicates, $n = 3$ biological replicates). $^{*}P < 0.05$, $^{**}P \leq 0.01$, $^{***}P \leq 0.001$, two-tailed Student's *t*-test. **b**, Western blot for AID protein expression in MEC1, Mino, JeKo-1 and GM06990 B-cell lines treated with the indicated inhibitors (1 μM) for 48 h. For comparison, Mino and GM06990 panels correspond to the panel shown in Fig. 4c and Extended Data Fig. 6d, respectively, with the addition of the ibrutinib lane ($n = 3$ biological replicates). For gel source data, see Supplementary Fig. 1. **c**, Histograms showing translocation junctions frequency to AID on-target and off-target sites in MEC1 and JeKo-1 B-cell lines treated with ibrutinib. For each treatment, data are from pooled HTGTS libraries of similar size from three independent experiments (Supplementary Tables 1, 4). Significance is calculated as FDR in ibrutinib over DMSO-treated human B cells. Statistical analysis is indicated in the Method. ***FDR ≤ 0.001. **d**, Mutation frequency of control non AID off-targets: intragenic regions for *PAX5*, *MTFR1*, *BCAT1*, *CLMN*, *UBXN7*, *ERICH6B* and random intergenic regions on chromosome 1, chromosome 8, and chromosome 18 were targeted re-sequenced in patients with CLL untreated or treated with idelalisib and ibrutinib. Box plots indicate cumulative frequencies of C-to-T or G-to-A transition mutation in DNA samples collected before (pre) and after (post) treatment in each patient (control, $n = 8$; idelalisib, $n = 10$; ibrutinib, $n = 10$; Supplementary Table 6). Whiskers extend to a maximum of 1.5× interquartile range beyond the box. *P* values calculated by paired samples two-tailed Student's *t*-test.